Received: 13 November 2019 | Revised: 21 October 2021 | Accepted: 22 October 2021

DOI: 10.1002/glia.24116

GLIA

WILEY

RESEARCH ARTICLE

Dystrophin deficiency affects human astrocyte properties and response to damage

Jenny Lange[1] | Olivia Gillham[1] | Reem Alkharji[1] | Simon Eaton[1] | Giulia Ferrari[2] | Monika Madej[3] | Michael Flower[4] | Francesco Saverio Tedesco[2,5,6] | Francesco Muntoni[5,7] | Patrizia Ferretti[1]

[1]Department of Developmental Biology and Cancer, Stem Cells and Regenerative Medicine Section, UCL Great Ormond Street Institute of Child Health, University College London, London, UK

[2]Department of Cell and Developmental Biology, University College London, London, UK

[3]Department of Neuromuscular Diseases, UCL Queen Square Institute of Neurology, London, UK

[4]UCL Queen Square Institute of Neurology, University College London, London, UK

[5]Dubowitz Neuromuscular Centre, UCL Great Ormond Street Institute of Child Health, University College London, London, UK

[6]The Francis Crick Institute, 1 Midland Road, London, UK

[7]NIHR Great Ormond Street Hospital Biomedical Research Centre, Great Ormond Street Institute of Child Health, University College London, & Great Ormond Street Hospital Trust, London, UK

Correspondence
Patrizia Ferretti, Department of Developmental Biology and Cancer - Stem Cells and Regenerative Medicine Section, UCL Great Ormond Street Institute of Child Health, University College London, London WC1N 1EH, UK.
Email: p.ferretti@ucl.ac.uk

Present address
Jenny Lange, UCL Great Ormond Street Institute of Child Health, University College London, Zayed Centre for Research into Rare Disease in Children, London, UK

Funding information
EBiSC, Grant/Award Number: 115582; European Research Council, Grant/Award Number: 759108; Medical Research Council (MRC), Grant/Award Number: G070089; National Institute for Health Research (NIHR) Great Ormond Street Hospital Biomedical Research Centre, Grant/Award Number: IS-BRC-1215-20012; Newlife Foundation for Disabled Children, Grant/Award Number: 15-16/12; National Institute for Health Research, Grant/Award Number: CL-2018-18-008; Saudi Arabian Cultural Bureau and Ministry of Education; The Wellcome Trust, Grant/Award Numbers: FC001002, GR082557

Abstract

In addition to progressive muscular degeneration due to dystrophin mutations, 1/3 of Duchenne muscular dystrophy (DMD) patients present cognitive deficits. However, there is currently an incomplete understanding about the function of the multiple dystrophin isoforms in human brains. Here, we tested the hypothesis that dystrophin deficiency affects glial function in DMD and could therefore contribute to neural impairment. We investigated human dystrophin isoform expression with development and differentiation and response to damage in human astrocytes from control and induced pluripotent stem cells from DMD patients. In control cells, short dystrophin isoforms were up-regulated with development and their expression levels changed differently upon neuronal and astrocytic differentiation, as well as in 2-dimensional versus 3-dimensional astrocyte cultures. All DMD-astrocytes tested displayed altered morphology, proliferative activity and AQP4 expression. Furthermore, they did not show any morphological change in response to inflammatory stimuli and their number was significantly lower as compared to stimulated healthy astrocytes. Finally, DMD-astrocytes appeared to be more sensitive than controls to oxidative damage as shown by their increased cell death. Behavioral and metabolic defects in DMD-astrocytes were consistent with gene pathway dysregulation shared by lines with different mutations as demonstrated by bulk RNA-seq analysis. Together, our DMD model provides evidence for altered astrocyte function in DMD

[Correction added on 22 November 2021, after first online publication: additional affiliation has been included for Francesco Saverio Tedesco and grant number has been updated for European Research Council]

suggesting that defective astrocyte responses may contribute to neural impairment and might provide additional potential therapeutic targets.

KEYWORDS
3-dimensional culture, astrocyte, brain, development, Duchenne muscular dystrophy, dystrophin, human, induced pluripotent stem cells, neural damage

1 | INTRODUCTION

Duchenne Muscular dystrophy (DMD), a progressive neuromuscular disease that affects 1 in 3000–5000 male children, leads to loss of ambulation by the early teens and death by the 3-4th decade of life (Blake et al., 2002; Muntoni et al., 2003; Ricotti et al., 2016). In addition to muscle wasting, and much less well understood, are the central nervous system comorbidities occurring in at least a third of DMD patients. These patients exhibit an IQ on average one standard deviation lower than the general population and suffer from a range of neuropsychiatric comorbidities including attention deficit hyperactivity disorder (ADHD) and autism (Pane et al., 2012; Ricotti et al., 2016; Wingeier et al., 2011). This research suggests that the incidence of the brain co-morbidities may be underreported, as borderline deficits occur in a larger proportion of DMD patients.

DMD is caused by mutations in the dystrophin gene, *DMD*, the largest gene in the human genome. *DMD* is composed of 79 exons and its expression is regulated by different promoters with distinct tissue specificity. It contains 3 promoter regions encoding full-length isoforms (Dp427) as well as at least 4 internal promoter regions encoding the shorter isoforms (Dp260, Dp140, Dp116 and Dp71/Dp40). All these shorter isoforms with possibly the exception of Dp116 are transcribed in the central nervous system (CNS) but not in muscle (Waite et al., 2012).

DMD individuals typically have intragenic loss of function mutations of the dystrophin gene, with the most frequent mutations being out-of-frame deletions (Aartsma-Rus et al., 2016; Juan-Mateu et al., 2015). All DMD mutations affect the expression of the full length dystrophin isoform, Dp427, produced both in muscle and in the brain. Genetic studies have clearly implicated a role for Dp427, Dp140 an Dp71 in the severity of the brain co-morbidities (Chaussenot et al., 2018; Hoogland et al., 2018; Pane et al., 2012; Ricotti et al., 2016).

The role of dystrophin has been extensively studied in muscle, where the full-length isoforms play an important structural role by connecting the cell cytoskeleton to the extracellular matrix (Blake et al., 2002). In contrast, relatively little is known about the role of the different isoforms in the brain, particularly in humans (Hoogland et al., 2018). It is still debated whether the neural deficits observed in DMD children are entirely acquired during prenatal development, hence "fixed," or there is some progression of the neural phenotype at least in the early years when the CNS is still highly plastic (Bagdatlioglu et al., 2020). Recent research has indicated differential expression of *DMD* transcripts between fetal and adult brain (Doorenweerd, Mahfouz, et al., 2017a); however, information on different dystrophin isoform expression in the developing human brain and in different neural cell types is still limited. More basic information on the expression of dystrophin isoforms in different human neural cells is required to develop a better understanding of how *DMD* mutations may affect human brain function. Dystrophin protein isoform analysis is challenging due to the complexity of this protein, with "new" dystrophin splice isoforms still being discovered, and to the low abundance of these proteins and transcripts (Aragon et al., 2018; Rani et al., 2019; Tadayoni et al., 2012).

Studies in a DMD mouse model lacking the full-length isoform have suggested a reduction in functional receptors at the GABAergic synapses, which is consistent with increased anxiety and fear responses observed in behavioral studies in these mice (Sekiguchi et al., 2009; Vaillend & Chaussenot, 2017). Altered distribution and clustering of synaptic proteins was also observed. In addition, mice lacking Dp71, which is expressed in various brain regions including neurons in the hippocampus, cortex and olfactory bulb, as well as in retinal and perivascular astrocytes, present several abnormalities (Aragon et al., 2018).

Astrocytes have been shown to play a role in the development of synaptic connections, and plasticity and homeostasis of neuronal circuits, for instance by modulating glutamate uptake (Pekny et al., 2016; Sofroniew & Vinters, 2010). Increasing evidence points towards a role for astrocytes in neuropsychiatric disorders including depression, in neurodegenerative disorders such as Alzheimer's disease and neurological disorders like epilepsy, which has high occurrence in DMD patients (Akther & Hirase, 2021; Hendriksen et al., 2018; Jones et al., 2017; Patel et al., 2019; Tsao & Mendell, 2006; van den Bergen et al., 2014). We therefore hypothesized that defects in astrocyte function may also contribute to the neural pathology of DMD.

Further knowledge of *DMD* expression in the developing human brain and of which cell types may be affected by dystrophin mutations is required to better understand the brain co-morbidities in DMD patients and eventually develop therapeutic strategies. Here we have addressed some of these issues, firstly by analyzing changes in dystrophin isoforms in the human developing brain and upon differentiation of human neural stem cells (hNSCs) into neurons and astrocytes, and secondly by testing the hypothesis that astrocytes derived from DMD

patient iPSCs (induced pluripotent stem cells) with mutations affecting several brain isoforms have functional deficits. We show that all shorter dystrophin isoforms are up-regulated with normal development, and that whilst neurons express most isoforms, Dp71 is the main isoform expressed in astrocytes. Importantly, we show for the first time that DMD astrocytes not only display morphological and molecular changes under basal conditions as compared to healthy controls, but also demonstrate altered response to inflammatory stimuli and oxidative stress. Our results highlight the importance of studying dystrophin expression in human neural cells, and point at a potential involvement of astrocytes in the observed brain co-morbidities in DMD patients.

2 | METHODS

All cell culture reagents were obtained from Life Technologies unless stated otherwise.

2.1 | Human tissues

All procedures involving human tissue were carried out in compliance with the UK Human Tissue Act 2006 with informed consent for study participation under ethical approval (NRES Committee London—Fulham, UK; REC: 18/LO/0822). Brains from three donors at 10, 15 and 19 post-conception week (pcw) fetuses were provided by the Human Developmental Biology Resource (HDBR, http://hdbr.org) tissue bank. Fibroblasts were obtained from the MRC Neuromuscular Diseases Biobank (UCL, London, UK; Research Ethics Committee reference no. 06/Q0406/33). Human cell work was conducted under the approval of the National Health Service (NHS) Health Research Authority Research Ethics Committee reference no. 13/LO/1826; Integrated Research Application System (IRAS) project no. 141100.

2.2 | Cell maintenance and differentiation

All cell lines and primary cultures were maintained in a humidified incubator at 37°C with 5% CO_2.

2.2.1 | Human neural stem cells (hNSCs) growth and differentiation in 2D (2 dimensional) and 3D (3 dimensional) cultures

hNSCs previously established from brains at Carnegie stages (CS) 17, 21 and 23, which correspond to embryonic week 6 (42–44 days), week 8 (53–54 days) and week 8 (56–60 days), respectively, were used (Sun et al., 2008; Kin Pong et al., 2014; Vagaska et al., 2016). They were grown in serum-free medium as previously described and passaged using Accutase (Kin Pong et al., 2014; Vagaska et al., 2016). All experiments were carried out using hNSCs between passages 10 and 20.

For astrocyte differentiation, hNSCs from all three Carnegie stages were passaged when at 80% confluency and plated directly into astrocyte differentiation medium consisting of DMEM/F12 medium with Glutamax supplemented with 1% P/S and 10% fetal bovine serum (FBS, Gibco). Astrocytes were cultured for a minimum of 3 weeks before commencing experiments with medium changes every 2–3 days. Astrocytes were plated at 6×10^5 cells/6 well plate for analysis by immunocytochemistry or western blotting.

Neuronal differentiation was induced by a growth factor removal protocol previously described with minor modifications (Sun et al., 2008; Vagaska et al., 2016). Briefly, hNSCs from the three different Carnegie stages (CS17, CS21 and CS23), were plated onto laminin coated 6-well plates (Corning) at 6×10^5 cells/plate. Cells were maintained in EGF free hNSC medium for 7 days, and then FGF2 and heparin were also withdrawn and hNSCs grown for a further 5 days. To allow maturation the cells were then grown for at least another 14 days in *BrainPhys* (Stemcell Technologies) with 1% P/S, BSA fraction 5, 1% N2 supplement, 2% B27 supplement, human brain derived nerve growth factor (BDNF, Peprotech) and human recombinant nerve growth factor (βNGF, Peprotech).

For 3D cultures, cells were mixed in hydrogels consisting of 1 mg/ml collagen I (Rat Tail High Concentration, Corning) and 2 mg/ml Matrigel (Corning) as described elsewhere (Vagaska et al., 2020) and allowed to polymerize for 40 min. In brief, a cold collagen I solution at pH to 7.4 was added to the Matrigel at 4°C before mixing the hydrogel with the cell suspension and inducing polymerization at 37°C for 30 min. In some experiments, hydrogels made of 100% collagen or 100% Matrigel were tested and different cell seeding protocols compared (Supplementary Figure 1). Astrocytes were differentiated for 3 weeks before being seeded into hydrogels, neurons were pre-differentiated for 14 days. Hydrogels were set in either 8 well chamber slides (50 μl with 1.5×10^4 cells per gel) or 6 well plates (500 μl with 1.5×10^5 cells per gel) and maintained for 5 days (hNSCs) or 14 days (astrocytes and neurons) before being fixed in 4% PFA for 30 min.

2.2.2 | Induced pluripotent stem cells (iPSCs) growth and astrocyte differentiation

iPSCs were grown on Matrigel-coated 6 well plates, maintained in mTESR1 medium (Stemcell Technologies) with 1% penicillin/streptomycin (P/S) (Life Technologies) and passaged using ReLESR (Stemcell Technologies). iPSC lines were generated using episomal reprogramming either in our laboratories (healthy controls 1 and 2, according to (Hawkins et al., 2016), and DMD68 (c.9851G > A [p.Trp3284X] in exon 68) by mRNA technology (Ferrari et al., 2020), or through the EBISC consortium (www.ebisc.org) and generated by Roslin Cell Sciences (DMD52: out-of-frame deletion; DMD67: c.9691C > T (p.Gln3231 in exon 67). The mutations carried by the DMD67 and DMD68 cell lines are expected to abolish the expression of all dystrophin isoforms, whereas the DMD52 line maintains

expression of Dp71 and Dp40, as the Dp71/Dp40 promoter is located in intron 63. A third healthy control line used exclusively for RNA-seq experiments was kindly provided by Professor S. Tabrizi (O'Regan et al., 2021).

To induce a neural progenitor fate, we used a protocol previously described (FitzPatrick et al., 2018). iPSCs were plated at 1×10^4 cells per well in u-bottom 96 well plates in neural induction medium supplemented with ROCKi. After 24 h, neuroepithelial clusters were visible and ROCKi was withdrawn. Daily medium changes were performed for 5 days after which the clusters were replated onto laminin coated 6 well plates. Neural rosettes were visible after 4 days, manually picked, centrifuged at 200*g* for 5 min and replated onto laminin coated plates in neural maintenance medium. These neural progenitor-like cells (NPCs) were expanded for a minimum of five passages before astrocyte differentiation was induced by directly plating NPCs into astrocyte differentiation medium as for hNSCs. These were maintained for a minimum of 3 weeks before further experiments. Astrocytes were plated at 1×10^4 cells/cm^2 for immunocytochemistry, cell viability and other assays.

2.3 | Protein extraction

Proteins were extracted from embryonic brains at 10, 15 and 19 pcw ($n = 3$ for each stage) from human fetal muscle at 20 pcw, and from wild type mouse brains (mouse protein extracts were kindly provided by S. Torelli). In brief, brain tissues mechanically dissociated in lysis buffer (4 M Urea, 125 mM Tris, 4% Sodium Dodecyl Sulfate) were shaken for 24 h at 4°C, before centrifuging the suspension for 15 min at 10,000*g*. To extract proteins from cell cultures, cells were rinsed with PBS and then lysis buffer added into the well. In some experiments, proteins were extracted with RIPA buffer (Sigma) for comparison. The cell lysate was kept at 4°C for 30 min and then centrifuged for 15 min at 10,000*g*. Protein concentrations were measured using the BCA assay kit (Thermofisher) according to the manufacturer's instructions; protein extracts were stored at −20°C until needed for western blot. Cells in 3D cultures were not analyzed by western blot due to interference of hydrogel proteins.

2.4 | Western blotting

After denaturing the protein extracts in sample buffer (Invitrogen) for 10 min at 70°C, 25 μg of protein per lane were loaded onto an Invitrogen NuPAGE 3–8% Tris-Acetate Gel and separated for 40 min at 75 V and then for approximately another hour at 150 V using a Xcell Sure Lock Mini-Cell (Life Technologies). HiMark Pre-Stained Protein Standard (31–460 kDa) and the Chamaleon Duo LI-COR ladder 8–260 kDa were used as size reference. Proteins were electrotransferred onto 45 μm PVDF membrane (30 V for two and a half hours on ice) using a transblot apparatus (Life Technologies). After confirming transfer by Ponceau red staining, membranes were incubated in blocking solution (1× Tris-buffered saline (TBS) with 0.5% Tween (TBS-T) and 10% semi-skimmed milk powder) for 1 h. Incubation with primary antibodies was overnight at 4°C and with secondary antibodies for 1 h at room temperature. All antibodies were diluted in in TBS-T containing 5% semi-skimmed milk powder. The antibodies used are listed in Table 1.

Bound antibodies were at first visualized using the Amersham ECL Western Blotting Detection system (GE Healthcare) kit and imaged on X-ray films (GE Healthcare) due to greater sensitivity in detecting dystrophin. For semi-quantitative analysis, Li-Cor Intercept Blocking Buffer and IRDye secondary antibodies were used and all Western blots were developed using an Odissey CLx (Li-Cor), band intensity was measured Li-Cor Image studio. Band intensity was normalized to house-keeping proteins (actin or GAPDH). Independent experiments were carried out at least 2 times, and most commonly, whenever sufficient material was available, in triplicates.

2.5 | Immunocytochemistry

All antibodies used are listed in Table S1. 2D and 3D cultures were fixed in paraformaldehyde (PFA) in phosphate-buffered saline (PBS, pH 7.4) at room temperature. After 1 hour in blocking buffer (10% Normal Donkey Serum/Normal Goat Serum and 0.1% Triton-X100 in PBS), cells were incubated overnight with the primary antibodies at 4°C and then with the secondary antibodies, together with Hoechst dye 33,258 (2 μg/ml) to counterstain the nuclei, for 1 h at room temperature. Negative controls were incubated with the secondary antibodies only. Images were acquired using either an Olympus IX71 inverted microscope with an ORCA-R2 digital camera (Hamamatsu Corporation, Bridgewater, NJ) or a confocal microscope (LSM710, Carl Zeiss, Jena, Germany). All images from immunostainings carried out at the same time and collected under the same conditions for comparison were analyzed with Fiji/Image J and/or Imaris software. Fluorescent intensity values were obtained by measuring intensity in 10 cells per image. Corrected total cell fluorescence intensity was obtained by multiplying the area of each selected cell by the mean fluorescence background reading and deducting this value for the integrated density. Analysis of cell morphology was performed as detailed below (Figure S2).

2.6 | Reverse transcription semi-quantitative PCR (RT-qPCR)

RNA was isolated using a RNeasy Mini kit (Qiagen) according to manufacturer's instructions. cDNA conversion was performed using RevertAid First Strand cDNA Synthesis kit (Thermo Fisher Scientific) also per manufacturer's instructions. cDNA was amplified either using the Taqman or SYBR-green method. Taqman Fast Advanced master mix (Thermo Fisher Scientific was used with Taqman probes for IL-6 (Hs00174131_m1) and VEGFA (Hs00900055_m1), alongside three housekeeping genes ATP5B (Hs00756996), EIF4A2 (Hs00756996_g1) and UBC (Hs00824723). The ΔΔCt method was applied to obtain the geometric mean of relative fold-change of data normalized to each

TABLE 1 Primary and secondary antibodies used

Target	Species	Supplier	Product Number
Primary antibodies			
Dystrophin (Dp (A))	rabbit	Abcam	Ab15277
Dystrophin (Dp (P))	rabbit	Proteintech	12715-1-AP
Dystrophin (4C7) Dystrophin MANEX1A[a]	Mouse	Santa Cruz Biotechnology	SC-33697
Dystrophin MANDYS1[a]	Mouse	From Morris	AB_528206
Dystrophin DYS2[a]	Mouse	Leica Biosystems	NCL-DYS2
Dystrophin MANDRA1[a]	Mouse	Abcam	ab7164
Actin	Rabbit	Sigma	A2668
MAP2	Mouse	Invitrogen	131500
SOX2	Rabbit	Millipore	Ab5603
Nestin	Rabbit	Millipore	ABD69
TBR2	Rabbit	Abcam	Ab23345
β3tubulin	Mouse	Promega	G712A
Vimentin	Mouse	Dako	GA630
GFAP	Rabbit	Chemicon	Ab5804
Glutamine synthetase	Mouse	Santa Cruz Biotechnology	SC-74430
Aquaporin 4	Rabbit	Abcam	ab46182
EAAT1	Rabbit	Abcam	ab41751
KI67	Rabbit	Abcam	Ab92742
BrdU	Rat	Serotech	MCA2060
Secondary antibodies			
Target	Host	Supplier	Product number
Rabbit	Goat	Invitrogen	A-11034 A-11037
Mouse IgG	Goat	Invitrogen	A-11029 A-11032
Rat	Goat	Invitrogen	A-11006 A-11007
Mouse	Goat	Li-Cor	926–68,070 926–32,210
Rabbit	Goat	Li-Cor	926–68,071 926–32,211

[a](Lam et al., 2014; Morris et al., 1995; http://www.glennmorris.org.uk/mabs/Dystrophin.htm).

reference gene. The QuantiTect SYBR Green master mix (QIAGEN) was used to amplify PADI2 (**Forward primer:** TGAAGCACTCGGAACACGT, **Reverse primer:** TTGTCACTGCTGGCCTCG) and the housekeeping gene RPL19 (L19) (**Forward primer**: GCGGAAGGGTACAGCCAAT, **Reverse primer**: CAGGCTGTGATACATGTGGCG). Three independent samples, each with technical triplicates, were amplified. The $\Delta\Delta C_t$ method was used to calculate the relative fold-change of data normalized to each reference.

2.7 | Astrocyte growth assay

Astrocytes derived from either healthy or DMD NPCs were plated at a density of 1.5×10^4 cells/cm^2 and 5′-bromo-2′-deoxyuridine (BrdU) (10 μM, Sigma) was added 2 days after plating for 24 h. Cells were fixed in 4% PFA for 10 min, washed 3 times in PBS and incubated at room temperature in 2 N hydrochloric acid for 20 min. The pH was then neutralized with 0.1 M borate buffer and cells were stained as described above with Ki67 and BrdU antibodies.

2.8 | Astrocyte functional assays

For all functional assays, astrocytes derived from either normal or DMD NPCs were plated at a density of 1.5×10^4 cells/cm^2 and experiments started by 3 days after plating to minimize possible bias due to differential growth.

The CellTiter-Glo 3D ATP assay (Promega) was used to measure production of ATP. Equal amounts of CellTiter-Glo reagent was added to the astrocyte medium and the cultures shaken for 5 min. After 25 min at room temperature, the luminescence was measured using a FLUOstar OPTIMA (BMG Labtech).

The 3-(4,5-Dimethylthiazol-2-yl)-2,5-diphenyltetrazolium bromide (MTT) reduction assay was used to assess astrocyte metabolic activity. Briefly, MTT (2.5 mg/ml) was added to astrocytes grown in 96 well plates and incubated for 2 h. After washing the cells with PBS, 200 μl dimethyl sulfoxide (DMSO) was added to each well and 100 μl of the supernatant was used to measure absorbance at 595 nm in a Thermo Scientific MultiSkan spectrophotometer.

2.8.1 | Glucose oxidation assay

Astrocyte glucose metabolism was measured using gas chromatography isotope-ratio mass spectrometry (GC-IRMS). Astrocytes were kept in experimental medium (glucose free DMEM with 15 mM HEPES, 2.9 mM sodium bicarbonate, 2 mM L-glutamine, 0.5 mM sodium pyruvate and 21.5 μM phenol red) supplemented with 10% FBS and 3 mM D-glucose for 20 h. Cells were washed with PBS and 3 ml experimental DMEM containing 3 mM [U-^{13}C] Glucose was added per well. To prevent the loss of $^{13}CO_2$ wells were sealed with a 3 ml layer of heavy mineral oil, and 100 μl samples were taken every hour for 6 h. Samples were stored in rubber-sealed Exetainer vials (Labco Ltd, Ceredigion, UK) and stored at −20°C until analysis. Once thawed, 100 μl 1 M hydrochloric acid was injected through the rubber lid to release $^{13}CO_2$. After centrifugation for 30 s at 500*g*, samples were analyzed on a GasBenchII linked to a Thermo Delta-XP isotope-ratio mass spectrometer (Thermo-Finnigan, Bremen, Germany).

2.8.2 | Astrocyte stimulation

For all stimulation assays, astrocytes derived from either normal or DMD NPCs were plated at a density of 1.5×10^4 cells/cm^2 and experiments started by 2 days after plating to minimize possible bias due to differential growth. Astrocytes were stimulated for 24 h.

LPS/IFNγ treatment

Astrocyte activation was induced by addition of lipopolysaccharides (LPS, 1 μg/ml, Sigma) and interferon γ (IFNγ, 90 ng/ml, Peprotech) to the astrocyte medium. Untreated and treated astrocytes were kept for 24 h following stimulation, after which they were fixed as previously described and stained for Vimentin and GFAP (glial fibrillary acidic protein). Astrocyte morphology (soma size) and cell number were measured as indicators of astrocyte response. Soma size was measured in sub-confluent cultures using ImageJ by manually outlining the soma of individual astrocytes excluding any processes (Figure S2); dividing cells were not measured. A minimum of 100 cells were measured per condition for soma size, and a minimum of 100 cells were counted per biological repeat in cell response experiments.

Oxidative stress induction

Oxidative stress was induced by adding hydrogen peroxide (H_2O_2) (Sigma) to the astrocytes for 1 h at different concentrations (from 0 to 500 μM), in FBS-free medium. Medium containing H_2O_2 was removed after 1 h and replaced with complete astrocyte medium, then cell viability was assessed after a further 24 h. To assess astrocyte viability following induction of oxidative stress, propidium Iodide (PI, 5 μg/ml) and Hoechst 33258 (2 μg/ml) were added to the cells. Cells were imaged using a 20× Zeiss objective to capture a large number of cells per field of view. Twenty random images were taken per biological replicate to quantify cell number and a minimum of 300 cells were counted per image.

2.9 | RNA-seq

RNA was extracted using a RNeasy mini kit (Qiagen) according to the manufacturer's instructions. One hundred ng of RNA per sample was used to generate RNA libraries by UCL Genomics. Each cDNA fragment was tagged with a sample specific sequence (index) and a unique molecular identifier (UMI). Samples were sequenced on the Illumina NextSeq 2000 that generated approximately 25 M reads/sample. Raw data was processed to remove poor quality base calls and contaminating Illumina adapter sequences. Reads that were shorter than 15 bases after trimming were discarded as these were considered too short to be mapped uniquely. Obtained reads were aligned to the human reference genome (GRCh38) with RNA Star. PCR duplicate reads were then removed using the mapping loci and the molecular identifier to ensure that a read is a true PCR duplicate. The raw count per transcript was then estimated. Additional quality control was performed to confirm that there was not excess ribosomal contamination. Transcripts per million (TPM) were obtained for 26,486 genes and FASTQ sequencing data were further processed in SARTools.

Differential expression analysis was performed on each of three control lines (2A, 12pcw, Hipsc) against each of two DMD lines (DMD52, DMD68) separately using SARTools package (DESeq2 wrapper). The primary analysis in this report tested whether there was differential expression between each DMD line and all control lines. This was done by combining the association p values for each gene using Brown's method which is essentially the Fisher's method for combining *p* values (Brown, 1975). The analyses were performed on three cell line comparisons, each DMD astrocyte line versus healthy 2A, 12pcw and Hipsc astrocytes; p values were Bonferroni corrected for three tests. This is conservative given that the disease groups are not independent. For comparison, p values were also combined using the Fisher's method (Dai et al., 2014) and the harmonic mean (Wilson, 2019). Log2fold change was combined by fixed effects meta-analysis to yield a standardized mean difference. These analyses were performed using a custom R script.

Gene Ontology (GO) enrichment analysis was performed using ShinyGo v0.66 (bioinformatics.sdstate.edu/go/) for Biological Processes, Cellular Components and Molecular Function on up- and down-regulated DEGs with Benjamin-Hochberg p-value correction of FDR < 0.05 for statistical significance. We examined the top 10 up- and down-regulated GO terms for each module in each DMD line and extracted terms enriched in both lines.

Kyoto Encyclopedia of Genes and Genomes (KEGG) Pathway analysis for Biological Processes was performed using Selection by iterative pathway group and network analysis looping (SIGNAL: https://signal.niaid.nih.gov/) (Katz et al., 2021) in up and down-regulated genes with $p < .05$. Log2Fold Changes were used as cut off values (Medium Confidence Cutoff Value >2, High Confidence Cutoff Value >7) and pathways were considered significantly enriched if the FDR was <0.05.

Metabolic Reaction Enrichment analysis (MAREA) was performed in GALAXY, using AREA4Galaxy (Damiani et al., 2020). Reaction Activity Scores (RAS) were calculated from TPM values for each DMD line and merged control lines using the Expression2RAS module. Here we used the HMRcore human metabolic network module which corresponds to the core model of central carbon metabolism (Damiani et al., 2017; Di Filippo et al., 2016; Graudenzi et al., 2018). The control RAS data set was then compared to each control line using the MAREA module. Differences between groups were considered significant if the *p*-value threshold determined by Kolmogorov–Smirnov test was <0.01 and the threshold fold-change was >1.2.

2.10 | Statistical analysis

For western blotting and experiments using hNSCs, 3 different cell lines with a minimum of 2 replicates each were assessed. In all metabolic experiments 6 repeats per cell line (3 DMD lines, 2 control lines) were included. Significant changes in protein levels, astrocyte growth, metabolic activity and response to damage were assessed either by Welch's *t*-test or one-way analysis of variance (ANOVA) with Bonferroni correction where appropriate using Graphpad Prism 7 software. Data are presented as mean ± SEM. A p value <.05 was considered significant. *: $p < .05$, **: $p < .01$, ***: $p < .001$, ****: $p < .0001$.

3 | RESULTS

3.1 | Dystrophin expression in human embryonic brain and neural cells

Expression of dystrophin isoforms in human neural tissue and cells was investigated using a number of antibodies binding to different regions of dystrophin, some of which have been widely used, though mainly in studies on muscle tissue (Figure S3). These included polyclonal antibodies, referred to here as Dp(A) and Dp(P) for simplicity, that were raised against epitopes in the C-terminus of dystrophin and in a sequence at the N-terminus of Dp71 shared by all isoforms, respectively, and a range of a monoclonal antibodies from Prof. Morris (http://www.glennmorris.org.uk/mabs/Dystrophin.htm). These had not been previously tested on developing human brain. MANEX1A, shown to recognize an epitope within the first 68 amino acids of dystrophin (Morris et al., 1995), hence referred to here as Dp1-68, appeared to recognize a high molecular weight band both in brain and muscle. However, in depth analysis of this band showed it could be resolved into two bands, with the larger one detected only in muscle, consistent with Dp427, and the smaller one in developing brain and muscle as well as neurones and astrocytes (Figure S4a). Based on analysis of expression in DMD68 cells, which lack all dystrophin isoforms (Figure S4b), this band appeared to represent a cross-reactivity of the antibody as it was present in both normal and DMD68 cells. Among other monoclonal antibodies tested, neither MANDYS1, which reacts with dystrophin rod domain and is expected to detect DP427 and Dp260, nor DYS2, which recognizes 17 amino acids at the C-terminus (Figure S4c), or MANDRA1 (Figure S5a) (Lam et al., 2014), which recognizes three amino acids within the C-terminus peptide used to raise Dp(A), displayed high sensitivity on brain proteins in western blots.

Hence, the widely used Dp (A), as well as Dp (P), were used to investigate dystrophin isoform expression during human embryonic development by western blotting in protein extracts from 9 human embryonic brain samples from 10, 15 and 19 pcw (Figure 1 A; $n = 3$ brains for each stage of development). Dp140 and Dp71 isoforms were highly expressed in the developing brain and recognized by both Dp (A) and Dp (P). The Dp(A) antibody reacted with all the expected dystrophin isoforms, and also with bands of approximately 40 and 30 kDa which may represent less widely investigated truncated dystrophin isoforms (some represented in Figure S3). Multiple bands detected for each isoform (e.g., both Dp140 and Dp71 appear as doublets) suggested occurrence of alternative splicing of dystrophin isoforms in fetal brains. Dp(P) displayed a more restricted staining profile, predominantly reacting with Dp140 and Dp71. Loss of immunoreactivity in DMD iPSCs, NPCs (neural progenitor cells) and astrocytes, not expected to express dystrophin proteins, confirmed the specificity of this antibody (Figure S6).

Low levels of expression of the full-length isoform, Dp427, were detected in developing brains by both the Dp(A) and Dp(P) antibodies by western blot at all stages tested (Figure 1a). Dp260 was not detected in any of the samples, consistent with this isoform being expressed predominantly in the retina. To semi-quantify expression of Dp140 and Dp71 during brain development, chemiluminescence of these protein bands was measured, and readings were normalized against β-actin expression. Comparable results were obtained with the two antibodies used. Both Dp140 and Dp71 significantly increased between 10 pcw and 19 pcw, providing evidence for a developmental up-regulation of these dystrophin isoforms in the human brain (Figure 1a). The intensity of the approximately 30 kDa band detected by Dp(A) in the developing brains did not change significantly (not shown).

In order to assess whether different isoforms detected in the developing brains were differentially expressed upon neural differentiation, we examined dystrophin expression using Dp(A) in three human

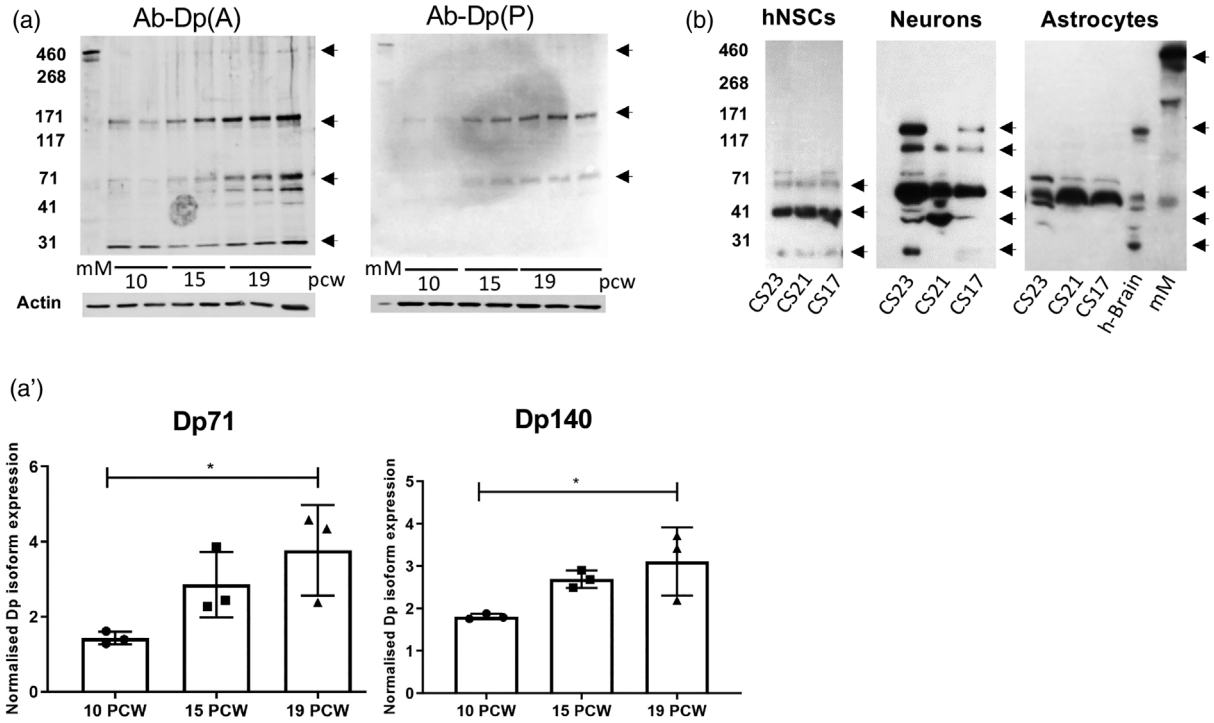

FIGURE 1 Dystrophin expression during human brain development and neural stem cell differentiation assessed by Western blotting. (a-a′) Western blots of protein extracts form 10, 15 and 19 post conception week (pcw) human fetuses with two different antibodies, Dp(A), from Abcam, and Dp(P) from Proteintech, that bind different regions of dystrophin C-terminus. Densitometric analysis of bands in the size range of Dp70 and Dp140 isoforms shows significant increase in these isoforms between 10 pcw and 19 pcw. Band intensity is normalized to β-Actin expression; numbers on the left indicate relative molecular weight of standard protein (kDA); arrowheads on the right indicate bands of the approximate size of dystrophin isoforms. mM, mouse muscle. $n = 3$ brains with 2 technical repeats. Data are presented as mean ± SEM and analyzed by one way ANOVA with Bonferroni correction. $p < .05$ *. (b) Western blots of protein extracts from human neural stem cells (hNSCs) from Carnegie stages (CS) 17, 21 and 23 and following their differentiation into neurons and astrocytes with the Dp(A) antibody. Human fetal brain (19 pcw, h-Brain) and mouse muscle (mM) are used as positive controls. Note differences in expression of the short isoforms in the different cell types; a band of approximately 30 kDa is visible in hNSCs and some neuronal cultures

neural stem cell (hNSC) lines derived from human brains at Carnegie stages (CS) 17, 21 and 23 and following their differentiation into neurons and astrocytes (Figure 1b). All hNSC lines expressed predominantly Dp40 and Dp71. Upon neuronal differentiation, Dp71 was the predominant isoform, but significant expression of Dp116 and Dp140 was also detected. A 30 kDa band was visible in hNSCs and in one of the neuronally differentiated lines. Astrocytes mainly expressed Dp71, with low levels of Dp427, Dp116 and Dp40 detected when increasing film exposure time (Figure S5b), whereas the 30 kDa band was not detected.

3.2 | 2D and 3D cultures for the analysis of dystrophin expression in human neural cells

Given the potential structural role of dystrophin in neural cells, we aimed to establish whether different cellular organization might affect its expression. To this purpose we compared dystrophin protein expression in 2-dimensional (2D) and 3D cultures (Figure 2).

A different response of hNSCs, neurons and astrocytes to the 3D culture environment was observed. hNSCs and neurons were evenly distributed throughout the collagen:Matrigel hydrogels (Figure 2a,b). In contrast, by 24–48 h after plating, astrocytes seeded under the same conditions consistently formed a thin layer at the bottom of the gel, with only a small number of cells remaining dispersed throughout it (Figure 2c). This distribution was not altered either by changing the stiffness of the gel using either 100% collagen or 100% Matrigel (data not shown) or by modifying the seeding protocol to exclude higher affinity of the astrocytes for the plastic rather than the hydrogel (Figure S1).

All three cell types were stained with Dp(A) antibodies both in 2D and 3D cultures (Figure 2). hNSCs grown in 2D or in 3D hydrogels were immunostained 5 days after seeding to avoid possible occurrence of spontaneous differentiation due to increased culture density; astrocytes were immunostained 21 days after seeding, and neurons were immunostained 14 days after growth factor withdrawal either in 2D or in 3D. Identity of the cells was confirmed by expression of typical markers associated with hNSCs (Nestin), neurons (MAP2, microtubule associate protein 2) and astrocytes (GFAP, glia fibrillary acidic protein) both in 2D and 3D (not shown). Strong Dp(A) staining was restricted to a subset of hNSCs both in 2D and 3D cultures (Figure 2a). In neuronally differentiated cultures, positive staining for Dp(A) was particularly evident in neuronal processes (Figure 2b). Upon

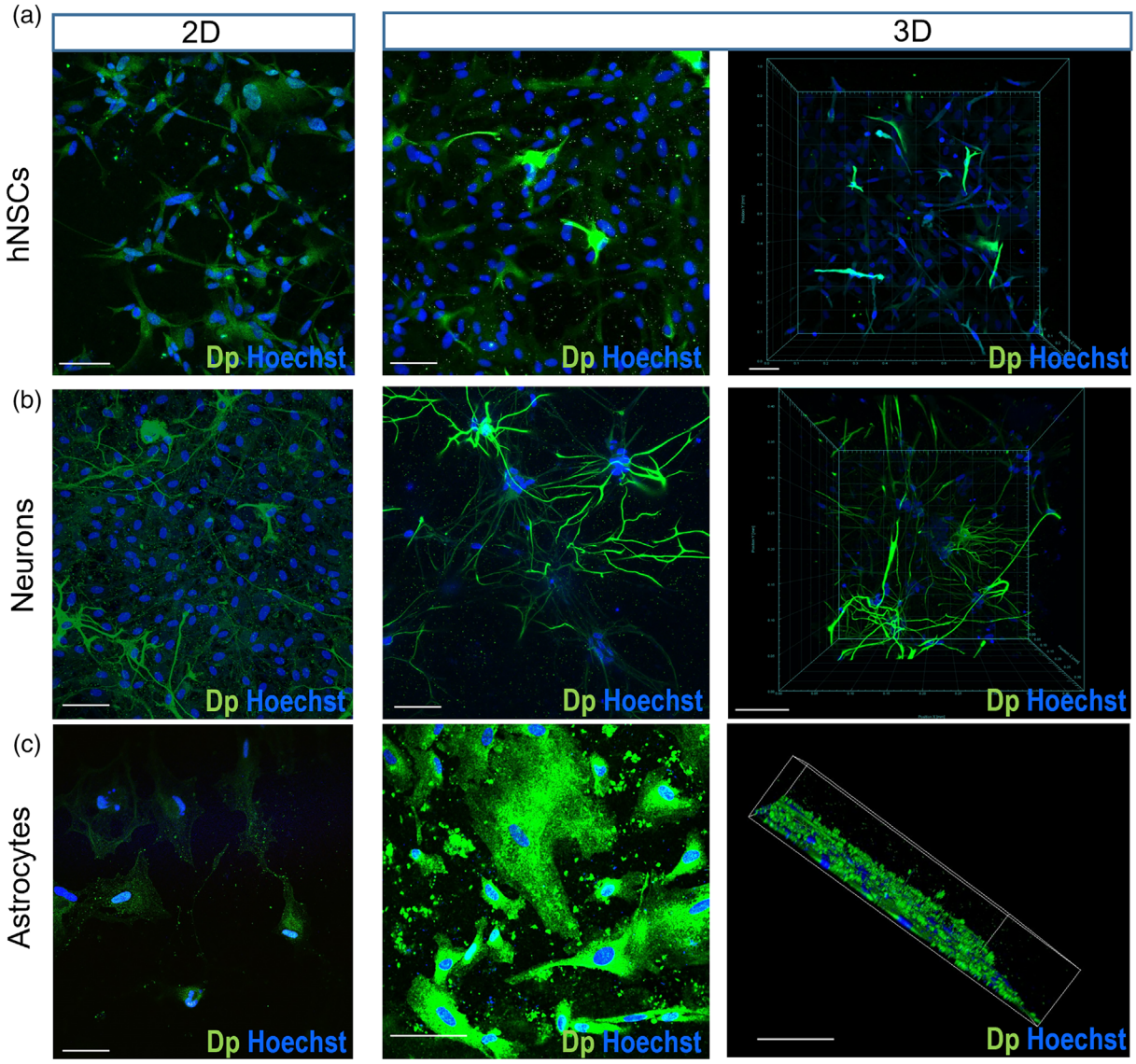

FIGURE 2 Dystrophin expression in human neural stem cells (hNSCs) and following their differentiation into neurons and astrocytes in 2D and 3D cultures. Cells are stained for dystrophin with the Dp(A) antibody (Dp) that detects all dystrophin isoforms (green). These are representative images of experiments carried out in 3 human cell lines from Carnegie stages 17,21 and 23 with 3 technical repeats. (a) hNSCs. Most hNSCs show some Dp expression, with a small number of strongly Dp-positive cells observed particularly in 3D culture. Note that in 3D culture cells are distributed throughout the hydrogel. (b) Neurons differentiated from hNSCs. Note a faint Dp staining in 2D neuronal cultures, whereas in 3D intense staining for Dp is observed in a subset of neurons. (c) Astrocytes differentiated from hNSCs. Note that only a faint staining for Dp is detected in 2D astrocytes; in 3D, astrocytes are strongly Dp-positive. Unlike hNSCs and neurons, astrocytes do not appear distributed throughout the gel. The left panel shows a 3D image of astrocytes in a hydrogel stained for Dp. Note that the majority of cells are layered at the bottom of the gel. All scale bars = 100 μM

astrocytic differentiation in 2D, Dp(A) was higher in neurons than in astrocytes. Differences in cellular localisation of dystrophin among neural cell types may reflect different cell-type specific roles.

3.3 | Differentiation of human iPSCs into astrocytes

The three DMD patient derived iPSC lines, DMD52, DMD67 and DMD68 and two healthy control iPSC lines were expanded and differentiated into neural progenitor cells (NPCs) and then into astrocytes as summarized in Figure 3a. Similar reactivity for a range of neural progenitor markers was observed in the 3 DMD cell lines, and examples of staining in DMD52 are shown in Figure 3b. Both control and DMD52 NPC lines displayed comparable expression profiles of neural stem cell markers, including SOX2 (>93%), Nestin (>95%) and Vimentin; TBR2, normally present in intermediate progenitor cells, was also expressed (Figure 3b, Supplementary Figure 7). GFAP, which is found in radial glia progenitors and astrocytes, was expressed in a small subset of NPCs (<10%). The neuronal marker MAP2 was also

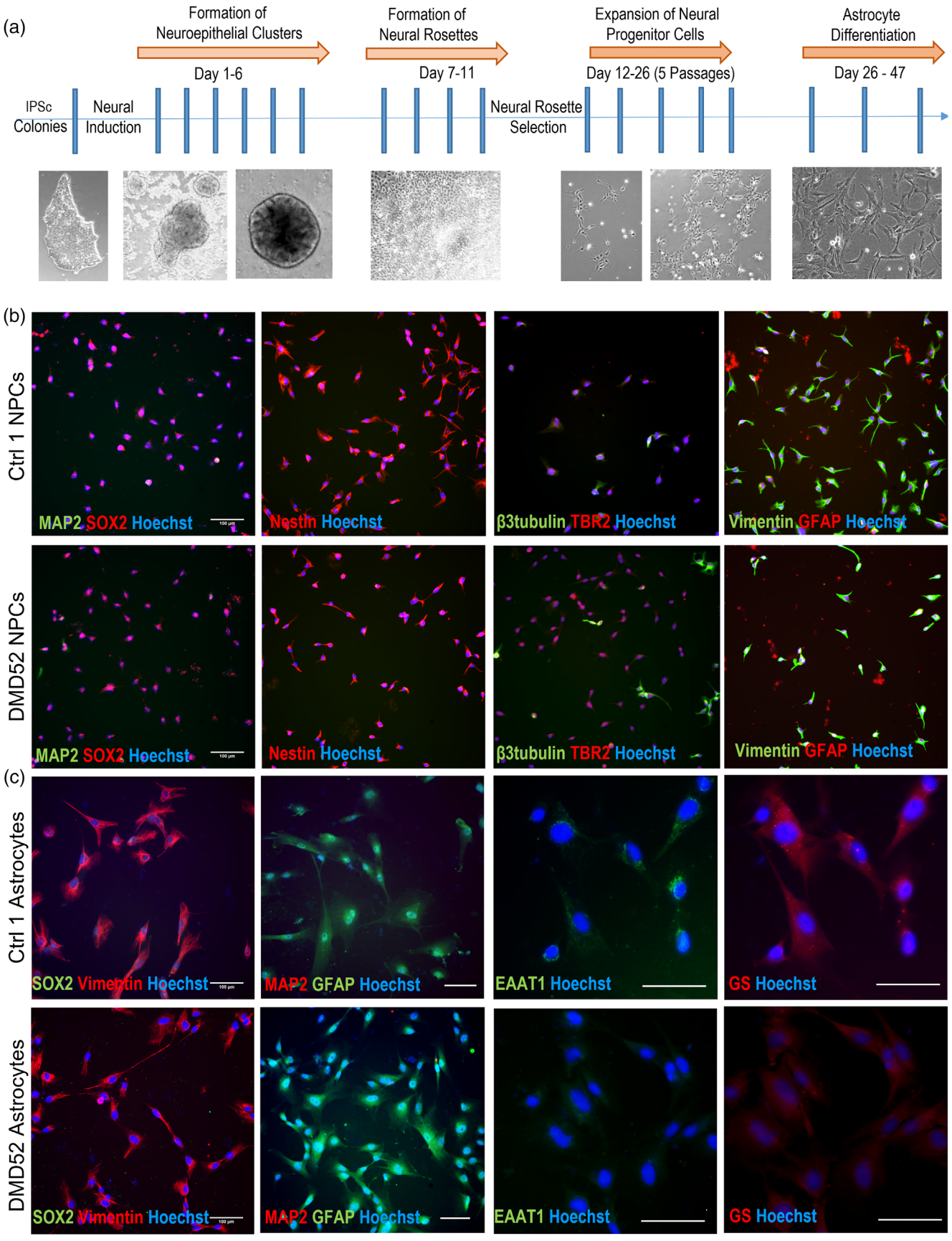

FIGURE 3 Legend on next page.

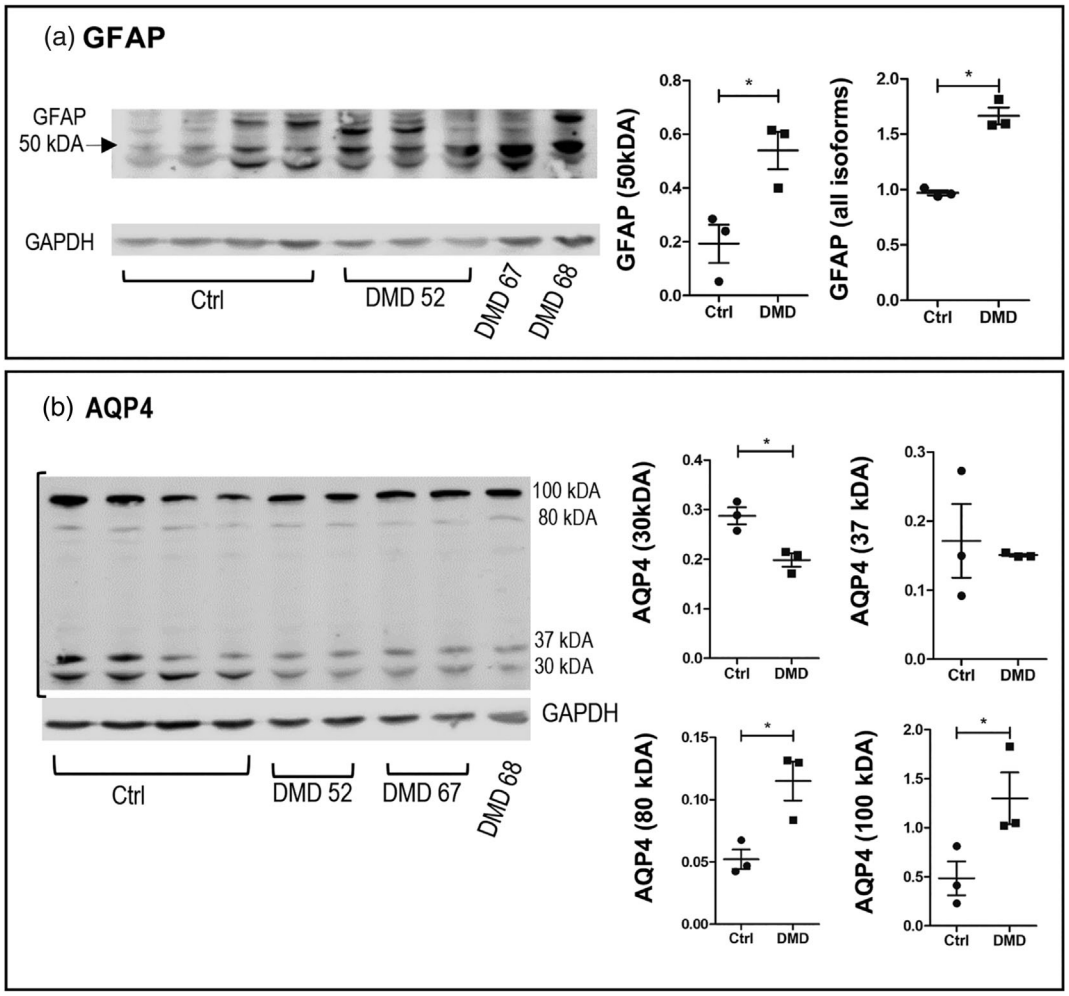

FIGURE 4 Glial Fibrilliary acidic protein (GFAP) and aquaporin 4 (AQP4) expression is altered in Duchenne muscular dystrophy (DMD) astrocytes. (a) GFAP detection by western blot. Note increased GFAP expression in DMD astrocytes as compared to control astrocytes (normalized to GAPDH). (b) AQP4 detection by western blot. Note that there is no difference in the expression of the 37 kDA isoform, whereas expression of the 30 kDa and of the large AQP4 (80–100 kDa, ubiquinated and tetrameric AQP4) isoforms is significantly reduced or increased, respectively, in DMD astrocytes as compared to controls (normalized to GAPDH). $N = 3$ DMD lines, $N = 2$ ctrl lines, 2 technical repeats. Data are presented as mean ± SEM and analyzed by Welch's t-test. *: $p < .05$

detected in a small subset of NPCs (<3%), and so was β3-tubulin (<6%). In contrast, O4, an oligodendrocyte lineage marker, was undetectable (not shown). It was also observed that SOX2 expression was reduced at later passages (~7 upwards) indicating a shift towards a more differentiated phenotype. No staining was detected when primary antibodies were omitted (Figure S8).

Astrocyte differentiation was assessed by immunofluorescence staining (Figure 3c and Figures S8 and S9). Again, the three DMD lines displayed a comparable behavior as compared to controls. Following astrocyte differentiation from NPCs (>P5) for a minimum of 3 weeks, all cell lines displayed a morphology resembling cultured astrocytes with over 99% of the differentiated cells expressing astrocyte markers, GFAP, vimentin, glutamine synthetase, GLAST/EAAT1 (excitatory amino acid transporter 1; Figures 3c and 4a,b and Figures S8 and S10). SOX2 expression was greatly reduced and, when still present, localized to the soma rather than the nucleus. No expression of

FIGURE 3 Generation of neural progenitor cells (NPCs) and astrocytes from control and Duchenne muscular dystrophy (DMD) iPSCs (induced pluripotent stem cells). Representative data (out of $N = 3$ for DMD lines, $N = 2$ control lines) shown here are for a healthy donor iPSC line (Ctrl) and the exon 52 mutation DMD iPSC line (DMD52). (a) Timeline of iPSC differentiation protocol. (b) NPCS from all lines express neural stem cell/radial glia markers, SOX2, TBR2, Nestin, vimentin and GFAP, but no (MAP2) or limited (β3-tubulin) amount of neuronal markers. (c) Control and DMD52 astrocytes. Note the change in morphology and loss of SOX2 upon differentiation. Expression of glutamine synthetase (GS), and of the excitatory amino acid transporter 1 (EAAT1) are detected in addition to GFAP and S100β. All scale bars = 100 μm

neuronal (MAP2, Figure 3b,c and Figure S7) and oligodendrocyte (O4, not shown) markers was detected. Together the staining pattern confirmed that healthy and DMD NPCs had undergone astrocytic differentiation, though a reduction in soma size was observed in the three DMD cell lines as exemplified in Figure S2 (see also Figure 6 and Figure S9). Furthermore, a significant reduction in EAAT1 staining was observed in all DMD astrocytes as compared to control astrocytes (Figure S10).

3.4 | Characterization of DMD astrocytes

DMD astrocytes were further characterized in the three DMD lines by assessing expression of a component of the astrocyte cytoskeleton, GFAP, and of Aquaporin 4 (AQP4), a protein expressed by astrocytes and known to be important in blood brain barrier function, by western blot. As dystrophin contains actin binding sites, we used expression of GAPDH to normalize protein expression in addition to expression of β-actin. Normalization to either house-keeping gene yielded similar results. While in the DMD astrocytes β-actin levels were not affected, GFAP was significantly higher than in controls (Figure 4a). Analysis of AQP4 showed that high molecular weight species (87 and 100 kDa), likely to be ubiquitinated AQP4 or AQP4 tetramers (Goodyear et al., 2008), were significantly increased in DMD astrocytes, whereas expression of the low molecular weight isoform (30 kDA) was significantly reduced compared to control astrocytes (Figure 4b) suggesting functional changes in AQP4 channels.

3.5 | Metabolic activity in healthy and DMD astrocytes

As astrocyte metabolic activity may have a substantial impact on neuronal health and homeostasis, we examined glucose oxidation in control and the three DMD astrocyte lines as an indicator of metabolic activity. The amount of glucose oxidized to CO_2 by astrocytes varied between cell lines, with slightly higher values in DMD than control astrocytes observed under basal conditions (Figure 5a). We then assessed astrocyte metabolism under basal condition by using an MTT assay and measuring ATP levels. Both assays showed a significantly increased metabolic activity in DMD astrocytes compared to control astrocytes (Figure 5b,c). To establish whether this increase primarily reflected increased cell number due to increased proliferation, expression of Ki67, a nuclear protein expressed at all stages of cell replication but not in quiescent cells, and BrdU incorporation were assessed (Figure 5d,e). Both were found to be higher in all three DMD astrocyte lines than in controls, but the fold change in BrdU incorporation (5.5%) and in Ki67-positive cells (29.2%) was lower than the over two-fold increase in MTT and ATP activity (Figure 5e). Furthermore, when the total cell number was counted 3 days after plating, there was no statistically significant difference between healthy and DMD astrocytes, though a trend towards a higher cell number in DMD was observed (Figure S10). This suggests that increased proliferation does not entirely account for the increase in metabolic activity detected with these assays under basal conditions.

3.6 | DMD astrocyte response to noxious stimuli

Given the morphological, molecular and growth differences observed in DMD astrocytes (Figures 5b–e and 6a, Figure S6), we investigated their function by exposing them to two types of stressors. One was exposure to LPS and IFNγ, which is commonly used to mimic inflammation and induces activation of primary astrocytes (Lange et al., 2018; Sheng et al., 2011), and the other exposure to H_2O_2 to induce oxidative stress (Figure 6).

Astrocyte morphology and changes in cell number were assessed under basal conditions and following LPS and IFNγ stimulation. Under basal conditions, astrocytes from the three DMD patient iPSCs were significantly smaller than healthy ones as indicated by Vimentin staining and measurement of soma size (Figure 6a,b). IFNy and LPS treatment did not induce any significant change in morphology, soma size or number of DMD astrocytes. In contrast, LPS/IFNy-treated healthy astrocytes exhibited a significant reduction in their soma size, though it still remained larger than in DMD astrocytes, and a 30% increase in number as expected upon stimulation. Hence it appears that DMD astrocytes do not respond normally to pro-inflammatory stimuli (Figure 6b).

The effect of oxidative stress induced by different H_2O_2 concentrations on cell survival was assessed by counting cell nuclei and propidium iodide (PI) positive cells (Figure 6c). A reduction in total astrocyte number was apparent at much lower H_2O_2 concentrations in DMD astrocyte cultures (from 100 μM) than in healthy astrocyte cultures (500 μM). Consistent with this observation, the percentage of PI positive cells was already significantly increased by 100 μm H_2O_2 in DMD but not in healthy astrocyte cultures. Furthermore, at 500 μm H_2O_2, cell death was significantly higher in DMD astrocytes than in controls. Together, the response to H_2O_2 observed suggests that DMD astrocytes are significantly more sensitive to oxidative stress than control astrocytes.

3.7 | Pathways affected in DMD astrocytes

In order to assess which are the pathways affected by dystrophin mutations that underpin the increased sensitivity to damage in DMD astrocytes, we compared astrocyte from three healthy lines, and the DMD52 and DMD68 lines by RNA-seq focusing on pathways affected in both DMD lines given the differences in isoforms affected in the two lines. Bulk RNA Sequencing provided expression data for 26,486 genes, of which 5657 genes were significantly up-regulated and 6527 genes were significantly down-regulated in both DMD52 and DMD68 astrocytes (Figure 7a). We performed GO enrichment analysis using ShinyGO (v0.66) and extracted the 10 most significantly enriched terms for each line (Table S1). Here we focus on terms that were significantly enriched in both DMD52 and DMD68 astrocytes

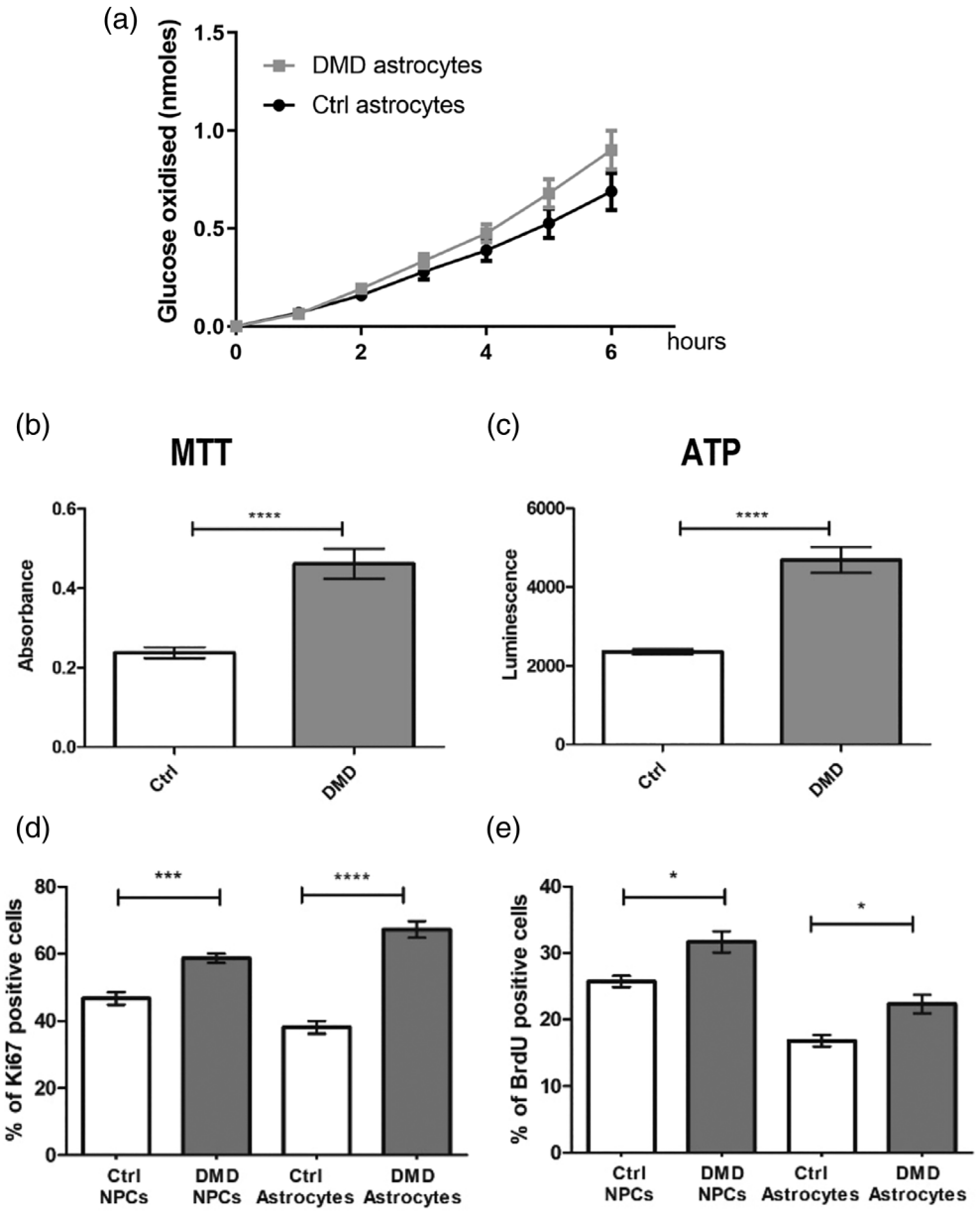

FIGURE 5 Metabolic and proliferative activity in control and Duchenne muscular dystrophy (DMD) neural progenitors (NPCs) and astrocytes. (a) Measurement of glucose oxidation by astrocytes every hour for 6 h does not show significant difference between DMD and control astrocytes. $N = 3$. (b) MTT assay. Significantly higher activity is observed in DMD astrocytes as compared to controls; $n = 3$, 6 technical repeats. (c) Measurement of ATP production by astrocytes shows a significant difference between controls and DMD astrocytes. $N = 3$, 6 technical repeats. (d) Percentage of NPCs and astrocytes labeled with the proliferation marker, Ki67. A higher percentage of Ki67-positive cells is present in DMD culture. (e) The percentage of cells synthesizing DNA (BrdU-positive) is also significantly higher in DMD cells compared to controls. (d and e) >100 cells were counted per technical repeat ($N = 3$ DMD lines, $N = 2$ ctrl lines, 3 technical repeats each). Data are presented as mean ± SEM and analyzed by Welch's *t*-test (b and c) or one way ANOVA with Bonferroni's correction (d and e). *: $p < .05$; ***: $p < .001$, ****: $p < .0001$

(Figure 7b–d). Significantly enriched terms included localization of proteins as well transport of proteins, peptides and amides, and up-regulation of genes involved in enzyme binding and transferase activity in DMD astrocytes. Terms associated with adhesion were also significantly enriched. The majority of down-regulated genes were associated with nervous system development, synaptic components and neuron differentiation, consistent with previous literature (Patel et al., 2019). Furthermore, GO terms associated with DNA binding were significantly enriched in down-regulated genes in DMD astrocytes.

We further examined pathways enriched in differentially expressed genes (DEGs) using the KEGG pathways analysis on the SIGNAL platform (Katz et al., 2021) (Figure 8). Consistent with our data suggesting that DMD astrocytes are in a reactive state, pathways enriched in up-regulated DEGs were linked to inflammation, such as TNF signaling, cytokine-cytokine receptor interaction, TGF-beta signaling and NF-kappa B signaling (Figure 8a). Furthermore, genes associated with glutathione metabolism were more highly expressed in DMD astrocytes, which is in line with our data showing that DMD astrocytes exhibit increased sensitivity to H_2O_2. The calcium signaling pathways featured for both up- and down-regulated DEGs, suggesting that calcium signaling in DMD astrocytes is highly disrupted. Synaptic pathways were enriched in down-regulated genes, consistent with reports from Patel et al (2020) (Figure 8b). We next generated heat maps for highly dysregulated pathways (Figures 9 and 10a, Figures S12 and S13), including PI3K-AKT signaling, pro-inflammatory pathways (cytokine-cytokine signaling, TNF signaling and NF-kB signaling) and calcium signaling. These show a large overlap of alterations in gene expression between the two DMD lines versus the controls. We further validated the RNA-seq

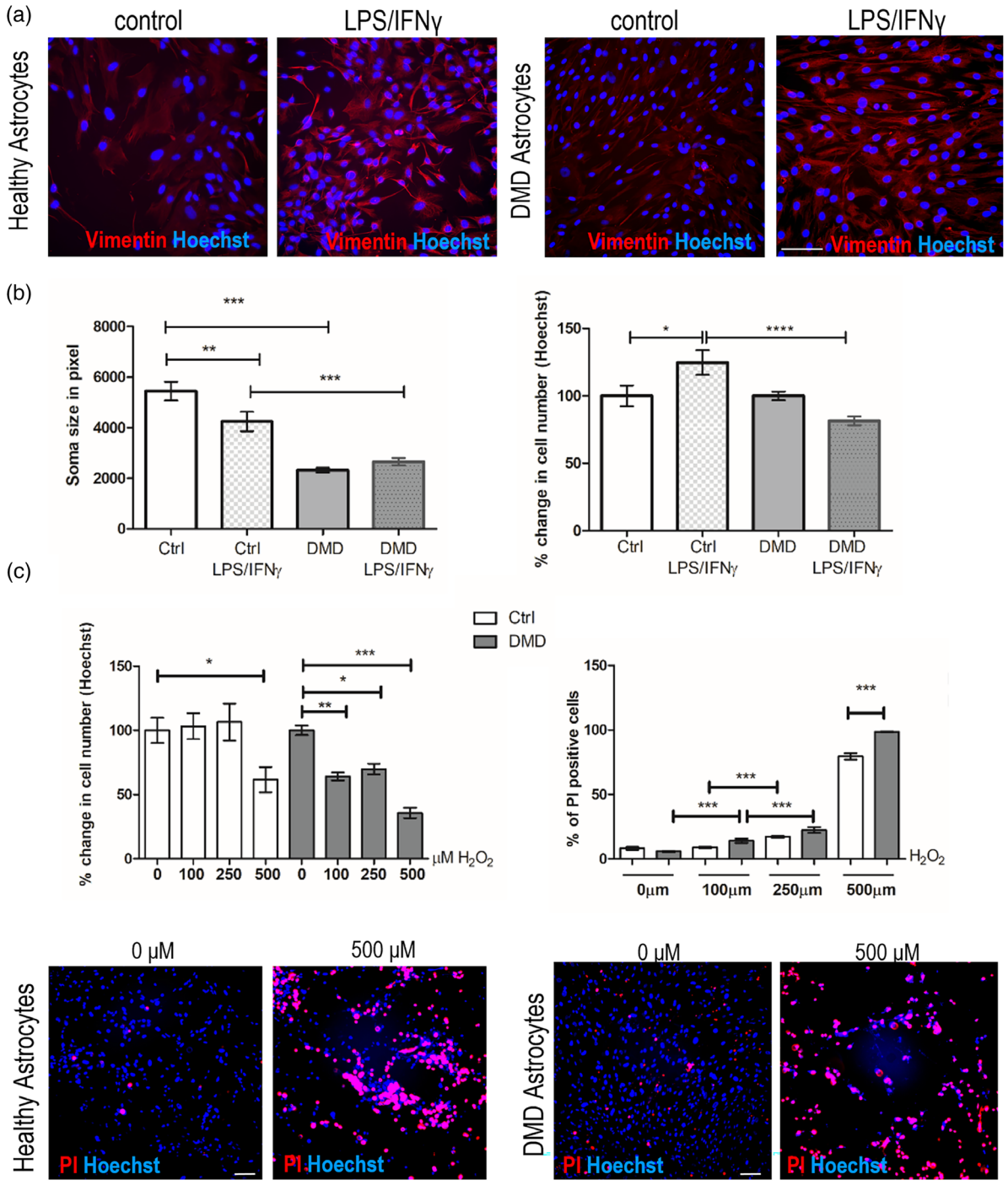

FIGURE 6 Inflammatory and oxidative stress response in control and Duchenne muscular dystrophy (DMD) astrocytes. (a) Vimentin staining (red) of unstimulated and LPS- and IFNγ-stimulated healthy and DMD astrocytes. Nuclei are stained with Hoechst dye (blue). Note that DMD astrocytes appear to be smaller than controls both under basal conditions and following stimulation with LPS and IFNγ for 24 h. $N = 3$ DMD lines, $N = 2$ healthy lines. (b) Measurement of soma size under basal conditions and following LPS/IFNγ and percentage of unstimulated astrocyte number following LPS/IFNγ treatment. Note that DMD astrocytes are significantly smaller than their healthy counterparts under basal conditions and following stimulation; significant reduction in soma size upon LPS/IFNγ stimulation is observed in healthy but not in DMD astrocytes. LPS/IFNγ stimulation increases the percentage of healthy but not DMD astrocytes. >100 cells were counted per condition, $N = 3$ DMD lines, $N = 2$ healthy lines. (c) Analysis of cell survival and death following induction of oxidative stress with hydrogen peroxide (H_2O_2) for 24 h in DMD and healthy astrocytes. Note that the percentage of cells present declines more rapidly with increasing concentration of H_2O_2 in DMD than in healthy astrocytes and a significant increase in dead cells, measured as percentage of nuclei (blue) that are propidium iodide (PI, red)-positive is already observed at 100 μM H_2O_2 in DMD astrocytes. >100 cells were counted per technical repeat (technical repeats: $N = 3$). Scalebar =100 μm. Data are presented as mean ± SEM and analyzed by one way ANOVA with Bonferroni's correction. *: $p < .05$; ***: $p < .001$ ***, ****: $p < .0001$

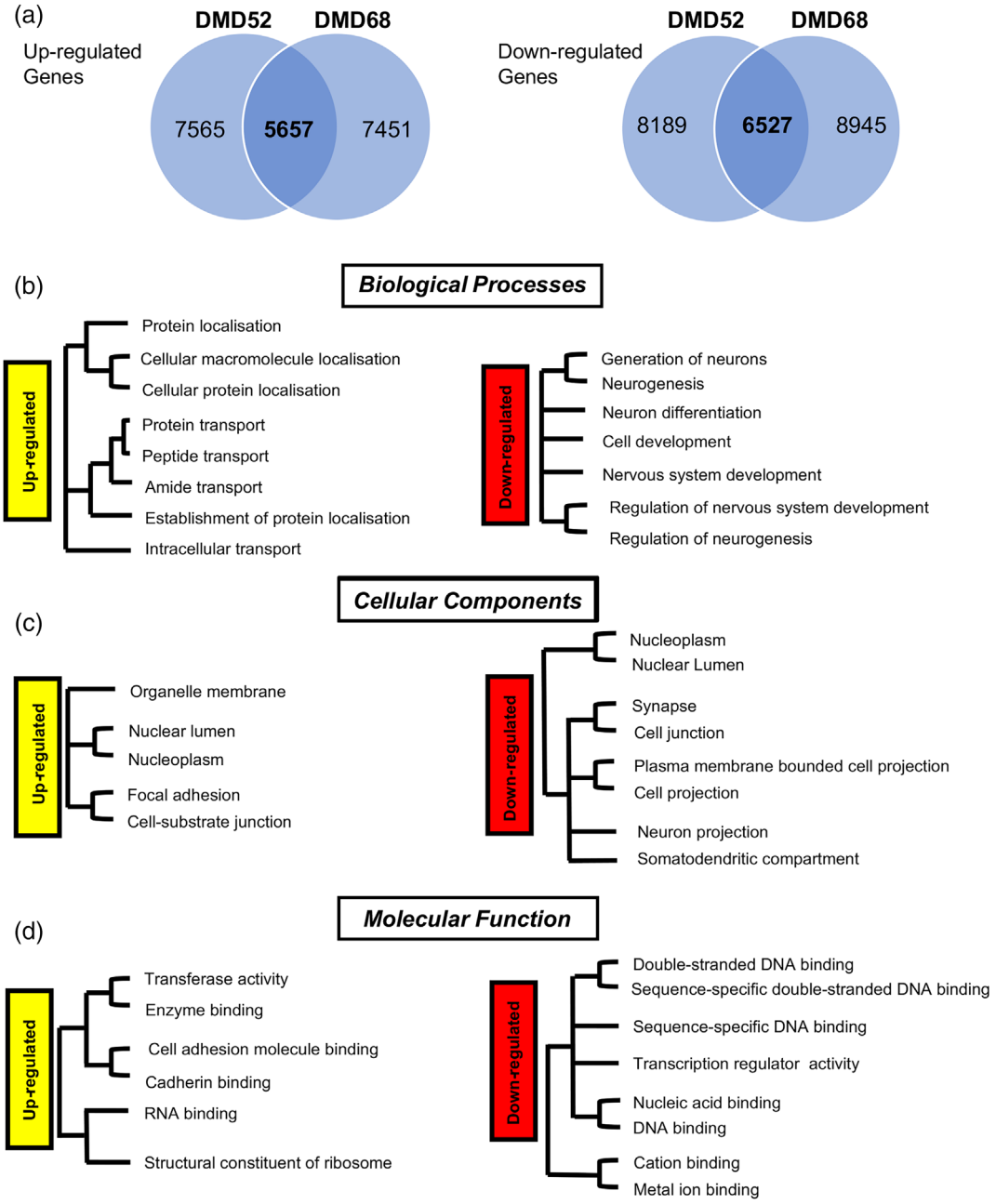

FIGURE 7 Gene ontology (GO) enrichment analysis reveals common pathways are disrupted in DMD52 and DMD68 astrocytes. (a) Venn diagram derived from analysis of bulk RNA sequencing of astrocytes from 3 control lines and two DMD lines (52 and 68): 5657 genes are found to be up-regulated and 6527 genes down-regulated in both DMD lines as compared to controls. (b–d) GO enrichment analysis shows up-regulation of genes involved in transport and localization, as well as binding, in astrocytes from both DMD lines. In contrast genes involved in neurogenesis, nervous system development and synapses are significantly down-regulated ($p < .01$)

data by assessing expression of some genes by RT-qPCR. Consistent with the RNA-seq changes, interleukin 6 (IL-6), vascular endothelia growth factor A (VEGFA) and the calcium-dependent enzyme, peptidyl-arginine deiminase 2 (PADI2) were found to be up-regulated in both DMD52 and DMD68 astrocytes (Figure 10b). Furthermore, according to RNA-seq analysis, *EAAT1* expression is down-regulated in DMD52 and DMD68 astrocytes, consistent with reduced EAAT1 protein expression assessed by immunofluorescence intensity data (Figure S10).

As we observed increased metabolic activity in DMD astrocytes, we performed metabolic reaction enrichment analysis (MAREA) (Damiani et al., 2020) focusing on carbon metabolism (Figure 11). Metabolic reactions involved in ornithine/arginine/citrulline mitochondrial transport were upregulated across both DMD astrocyte lines, as well as phosphoenolpyruvate carboxykinase, a key enzyme of gluconeogenesis, folate metabolism and H_2O metabolism. Metabolic reactions involved in fatty acid metabolism were upregulated in both lines, although this was more extensive in DMD68

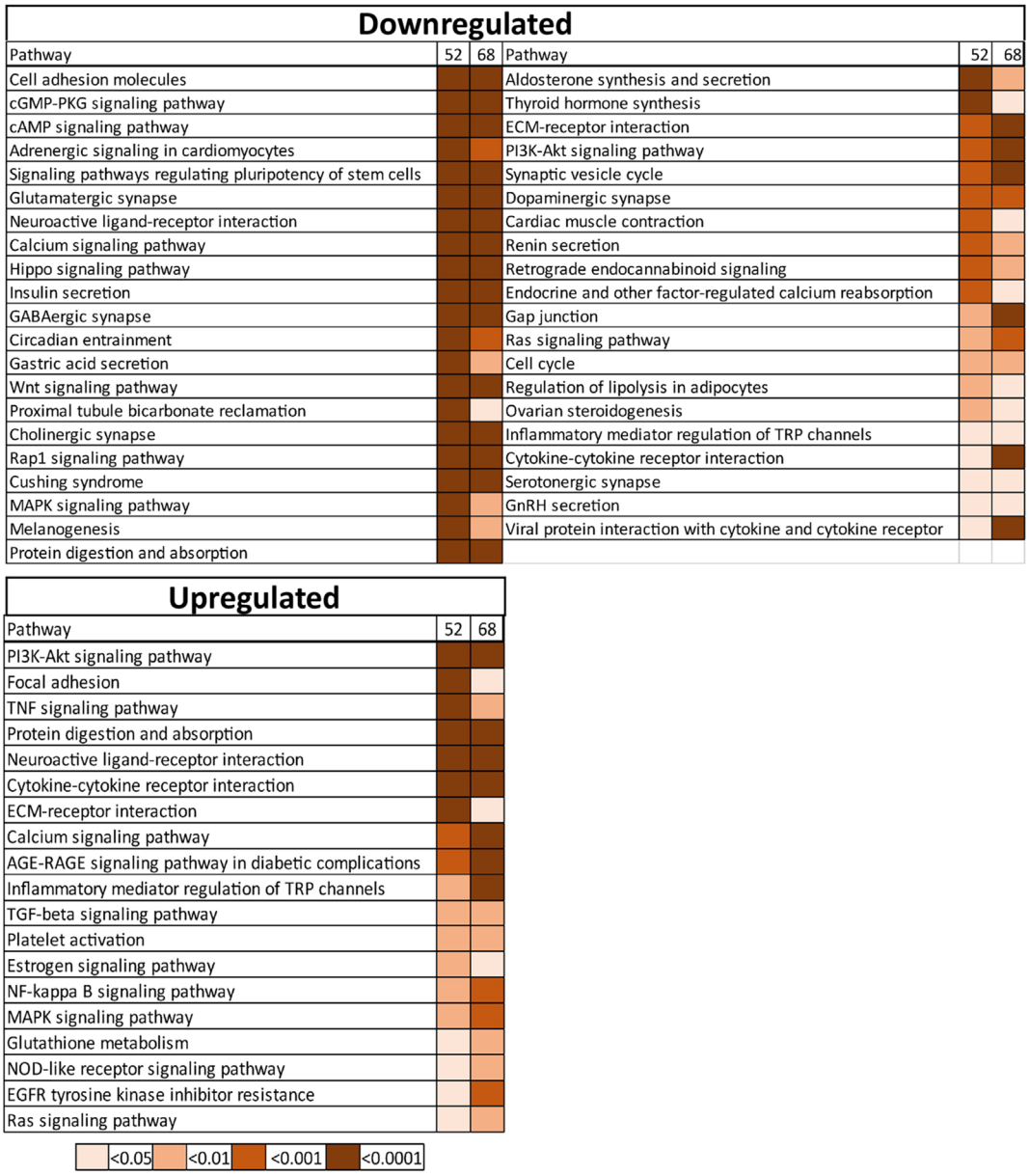

FIGURE 8 Kyoto encyclopedia of genes and genomes (KEGG) pathway analysis highlights up-regulation of pro-inflammatory pathways in DMD astrocytes. List of down-regulated and up-regulated pathways with Log2Fold changes >2 and FDR < 0.05 that have been extracted from KEGG pathway analysis for each line and are enriched in both DMD52 (52) and DMD68 (68) astrocytes. Note enrichment of several pro-inflammatory pathways in both DMD astrocytes; glutathione metabolism is also significantly up-regulated; pathways involved in astrocyte function, such as calcium signaling, are highly dysregulated and pathways involved in synapses are significantly down-regulated

astrocytes. MAREA analysis confirms that metabolic reactions are upregulated in DMD astrocytes, though to a greater extent in DMD68 astrocytes.

4 | DISCUSSION

Here we have reported changes in dystrophin protein expression in the human developing brain and in human neural progenitors and their progeny, and importantly shown that the phenotype, metabolism and injury response of astrocytes from DMD patients are altered, consistent with very recent observations (Patel et al., 2019).

4.1 | Expression of the smaller isoforms of dystrophin increases with development

Low levels of Dp427 protein were observed at early and mid-fetal stages of human brain development and are consistent with a recent analysis of dystrophin expression at the transcriptional level

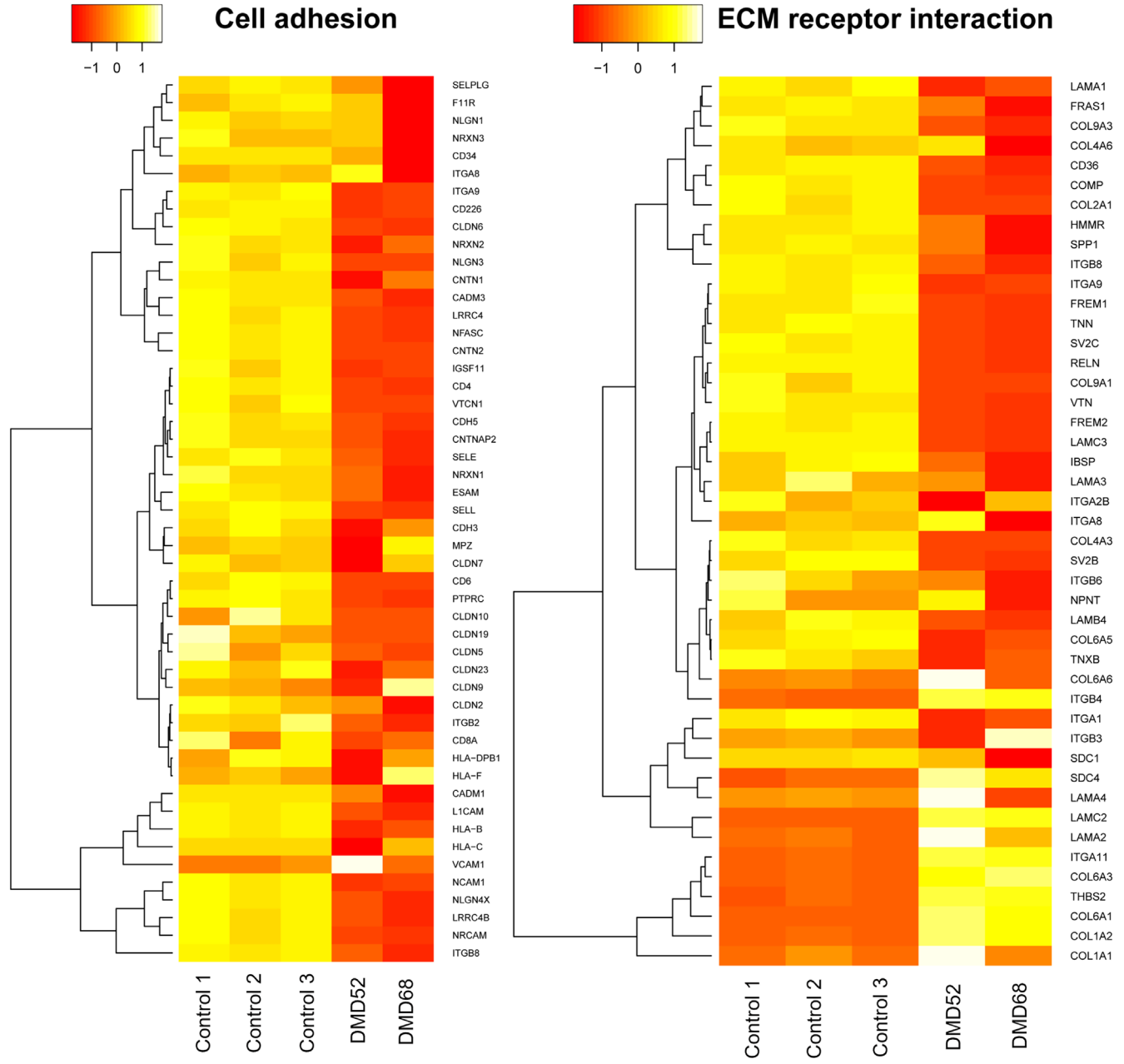

FIGURE 9 Heatmaps show significant down-regulation of genes involved in cell adhesion and extracellular matrix (ECM) receptor interaction. Hierarchical clustering of differentially expressed genes (DEGs) shows significant down-regulation of genes involved in cell adhesion and ECM receptor interaction between DMD astrocytes and control astrocytes

(Doorenweerd, Mahfouz, et al., 2017b). In contrast, we found expression of Dp140 and Dp71 proteins at 10, 15 and 19 pcw with clear up-regulation between 10 and 19 pcw, which had not been previously highlighted by the mRNA analysis. This is likely due to the fact that the study published by Doreenweerd et al. (2017) focused on mRNA expression, while ours analyzed protein expression, as well as other differences in experimental design. Of particular importance, we have analyzed three brains for each developmental stage separately, and did not pool different stages. Furthermore, because of probe availability, the transcriptional analysis carried out by Doreenweerd et al. (2017) did not allow for individual assessment of the Dp71 and Dp40 isoforms (transcribed by the same promoter), whereas different short isoforms can be detected on the basis of their different molecular weight by western blotting. Depending on the neural cell type, Dp (A) reacted also with bands of approximately 30 kDa and/or 40 kDa. Importantly, Dp (A) does not recognize a micro-dystrophin that lacks the C-terminus, thus demonstrating specificity (Montanaro, personal communication). Interestingly, bands of similar sizes have been observed in western blots for dystrophin in human and rat brains in other studies, though this was not commented on by the authors (Hendriksen et al., 2016; Hoogland et al., 2018). There is evidence for several short Dp71 variants that contain the C-terminus, including a

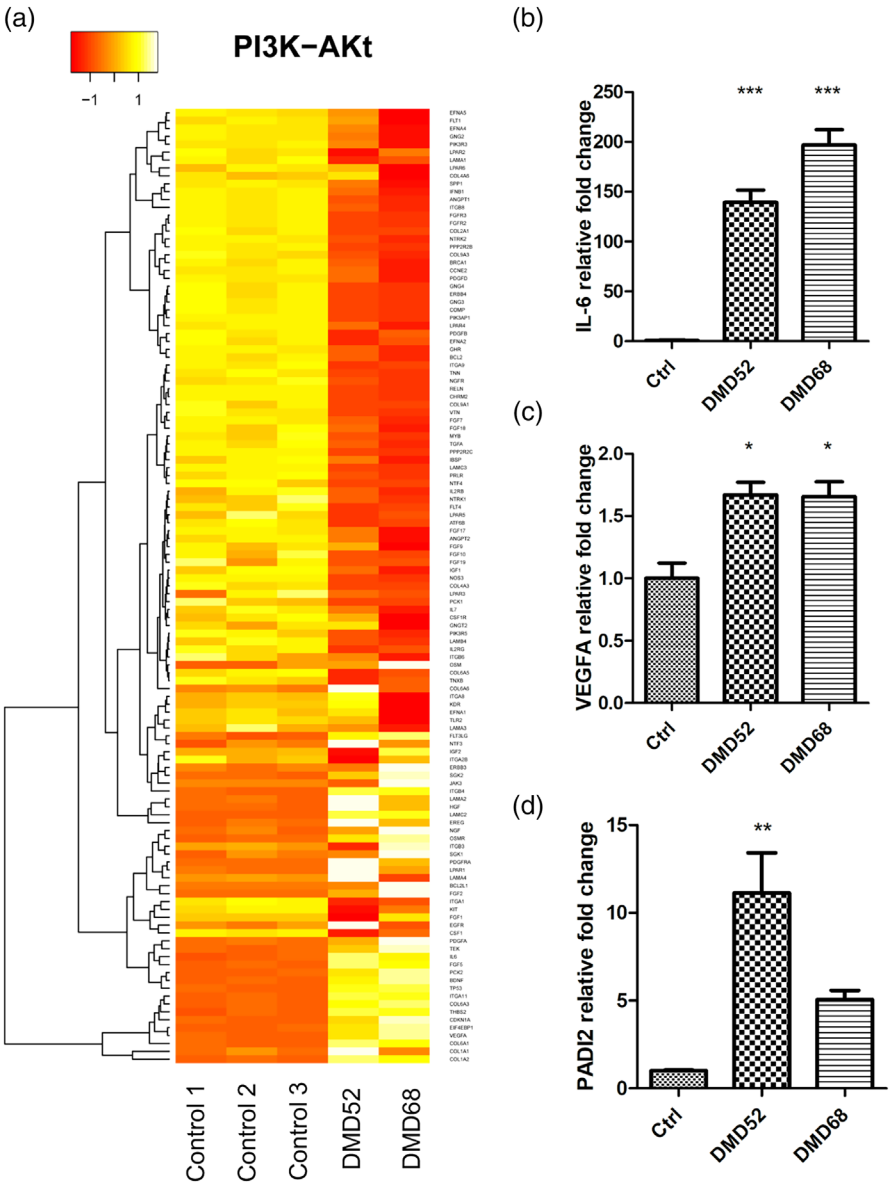

FIGURE 10 Heatmap of genes involved in PI3K-AKT signaling and validation of differentially expressed genes by RT-qPCR. (a) Hierarchical clustering of differentially expressed genes (DEGs) shows dysregulation of key genes involved in PI3K-AKT signaling in DMD astrocytes, with a greater number of significantly up-regulated than down-regulated genes in both DMD52 and DMD68 astrocytes. (b–d) analysis of differentially-expressed genes by RT-qPCR is consistent with RNA-seq data, as exemplified by up-regulation of interleukin 6 (IL-6), vascular endothelia growth factor A (VEGFA) and the calcium-dependent enzyme, peptidyl-arginine deiminase 2 (PADI2) in DMD astrocytes

novel variant consisting of 216 amino acids, with an estimated 24.8 kDa molecular weight recently identified in glioblastoma (Rani et al., 2019).

While our use of different antibodies has provided consistent results on the expression of the better characterized isoforms in human neural cells and developing brains, the complexity of the dystrophin protein variants, together with a limited number of studies showing full western blots and/or focusing on human neural tissues, calls for future in-depth characterization of the putative small dystrophin isoforms and their alternative splicing in the brain. Research on DMD has so far focused mainly on the muscle, but as it is increasingly extending to other human tissues, including brain, retina and heart, and to dystrophin role in development. Hence, antibody characterization will need to be further broadened to these tissues with a greater emphasis on the complexity of dystrophin isoforms, newly emerging ones and potential roles of dystrophin products, as well as careful analysis of potential cross-reactivities, as exemplified by our unexpected finding of MANEX1A reactivity with "non-dystrophin" protein(s) both in developing muscle and brain (Barnabei et al., 2015; Fujimoto et al., 2017; Kawaguchi et al., 2018; Morris et al., 1995; van den Bergen et al., 2014).

Together, the predominance and developmental regulation of small dystrophin isoforms in early fetal brains, and published studies showing association of mutations in Dp140 and Dp71 with brain comorbidities, is consistent with the hypothesis that these deficits are largely due to developmental abnormalities, and not purely progressive as in the muscle (Bagdatlioglu et al., 2020; Chaussenot et al., 2018; Hoogland et al., 2018; Muntoni et al., 2003). Given the plasticity of the young brain, it is conceivable they could be ameliorated by early intervention. Significantly, in the mdx mouse an antisense oligonucleotide treatment that induced expression of a truncated dystrophin form with some functional activity improved their emotional/cognitive responses (Relizani et al., 2017).

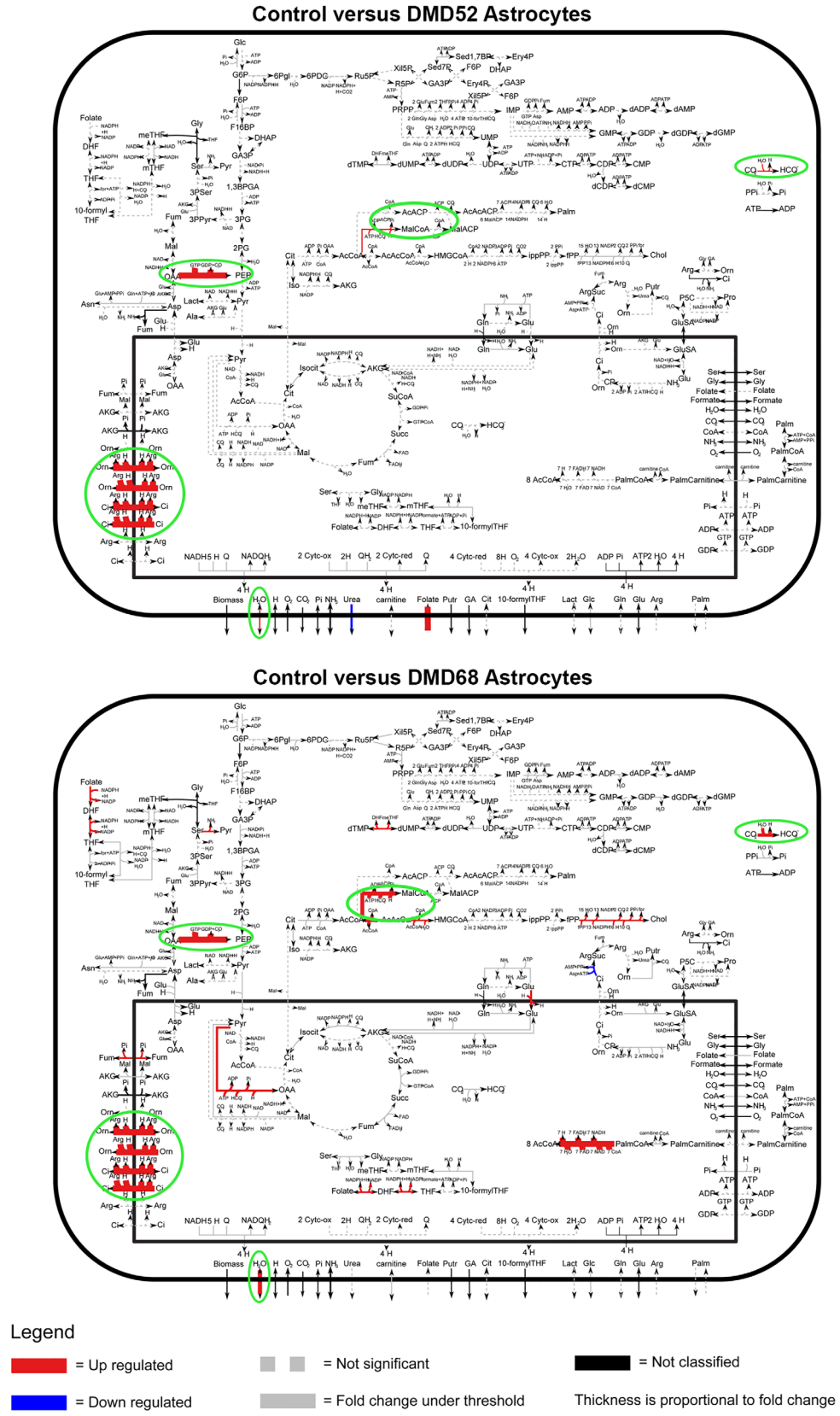

FIGURE 11 Metabolic reaction enrichment analysis (MaREA) highlights metabolic up-regulation in DMD52 and DMD68 astrocytes. HMRcore map enriched by MaREA analysis, up-regulated reactions are marked in red, down-regulated reactions are marked in blue. Thickness in arrows reflect log2 fold changes, reactions were considered significantly enriched if $p < .05$ by non-parametric Kolmogorov–Smirnov test. Several metabolic reactions are highly enriched in both DMD52 and DMD68 astrocytes

4.2 | Dystrophin is differently regulated in neurons and astrocytes upon neural progenitor cell differentiation

Analysis of dystrophin expression by western blot in hNSCs and following their differentiation into neurons and astrocytes indicated cell type-specific regulation of dystrophin isoforms. In astrocytes Dp71 was the main up-regulated isoform, whereas in neurons Dp140 and Dp116 were also clearly visible. Detection of Dp116 was unexpected, as within the nervous system expression of this isoform has been reported only in Schwann cells and in glioblastoma-derived cells (Mahyoob Rani et al., 2019; Matsuo et al., 2017). The full-length dystrophin was also more readily detected in hNSCs and neurons than in astrocytes. Expression of Dp71 in human astrocytes is consistent with its reported expression in rat and mouse astrocytes (Giocanti-Auregan et al., 2016; Imamura & Ozawa, 1998). The distinct dystrophin profiles between neural cell types is consistent with the findings that *DMD* mutations disrupting distinct isoforms may differentially impact brain function in DMD patients (Blake et al., 2002; Muntoni et al., 2003; Ricotti et al., 2016).

Another parameter that affected dystrophin expression was culture dimensionality, as differences in dystrophin staining were observed when hNSCs, neurons and astrocytes were grown in 3D as compared to 2D cultures. Nonetheless, the antibodies used allowed comparison of full-length dystrophin against all isoforms and further highlighted different pattern of expression among neural cell types. Culturing astrocytes in 3D appeared to greatly increase dystrophin staining. Based on the western blot results, this most likely reflects expression of Dp71 in astrocytes. Given the known structural role of dystrophin in muscle, the changes observed here between 2D and 3D support an important structural role for dystrophin also in the nervous system.

4.3 | DMD mutations affect astrocyte phenotype and function

The DMD patients from whose cells the iPSCs were generated carried different mutations, with two of them anticipated to affect all isoforms, including Dp427, Dp140, Dp71 and Dp40 (DM67 and DM68), and one (DMD52) expected to affect the larger isoforms, but not Dp71 and Dp40 (Ferrari et al., 2020). Defects in Dp71 have been proposed to contribute to neural impairment in patients as well as in animal models (Chaussenot et al., 2018; Daoud et al., 2009). Most recently Patel et al. (2019) have shown that mutations affecting the full-length isoform are sufficient to disrupt homeostatic activity of astrocytes and affect neuronal health. This is consistent with our findings that there are not notable differences in astrocytic responses between the patient lines studied, all lacking a functional full-length isoform, but with short isoforms differently affected.

Although expression of classical astrocytic markers indicated that DMD-iPSCs could generate astrocytes, they presented morphological abnormalities that were independent of the dystrophin mutation carried. Furthermore, GFAP protein expression was significantly increased in all our DMD astrocytes, which is consistent with the up-regulation of GFAP transcripts in DMD astrocytes also recently reported (Patel et al., 2019). Importantly, GFAP up-regulation is a feature of reactive astrocytes. Several studies in mouse (Annese et al., 2016; Nico et al., 2004) also suggested alterations in blood brain barrier astrocytes and reported a decrease in the expression of the 30 kDa form of AQP4, a water-selective membrane channels that plays a key role in maintaining water homeostasis in the brain (Frigeri et al., 2001; Nico et al., 2004). In our human DMD astrocytes we observed a shift from the short AQP4 isoforms, where expression was significantly lower than in control astrocytes, to a significant increase in ubiquitinated AQP4 (87 and 100 kb). Changes in astrocytic GFAP and AQP4 are likely to disrupt astrocyte function and responses in humans, hence impacting upon blood–brain barrier function as proposed in the *mdx* mouse brain and in the Dp71 null mouse retina (Frigeri et al., 2001; Giocanti-Auregan et al., 2016; Li et al., 2020). Interestingly, astrocyte abnormalities and a reduction in AQP4 and Dp71 levels have been reported in post-mortem studies of patients with idiopathic normal pressure hydrocephalus (Eide & Hansson, 2017). While defective cerebral perfusion in DMD patients has recently been reported, studies on blood–brain barrier function in these patients are still missing and will be valuable to further understanding of the DMD neural pathology (Doorenweerd, Dumas, et al., 2017).

As astrocytes play a crucial role in brain function, changes in their properties may have a substantial impact on neuronal homeostasis and response to damage (Belanger et al., 2011; Pekny & Pekna, 2014). Recently, defects in glutamate clearance and changes in Ca^{2+} homeostasis in DMD astrocytes carrying different mutations have been shown to contribute to neurotoxicity, which was alleviated through restoration of dystrophin function and defects in glutamate handling were mainly attributed to lack of Dp427 (Patel et al., 2019). The DMD astrocytes investigated in that study did not show differences in population doublings. In contrast, under basal conditions, astrocytes from the DMD iPSCs studied here displayed significantly higher BrdU incorporation and Ki67 expression than controls, though the total cell number at the time point investigated was not significantly different. Hence the increase in metabolic activity detected by the MTT and ATP assays in DMD astrocytes under basal conditions may not be fully due to higher proliferative activity. Together, increased DNA synthesis and metabolic activity in DMD astrocytes as well as their raised GFAP expression and morphological changes are consistent with patient-derived astrocytes being in a more activated state than healthy astrocytes.

While analysis of glucose oxidation under basal conditions revealed an upward trend in DMD astrocytes as compared to control healthy ones, more variability between both healthy and DMD lines was observed in this parameter than in any other studied. In contrast, upon exposure to stressors, differences in cellular responses between DMD and healthy astrocytes were clearly evident in all lines. Stimulation with LPS/IFNy, commonly used to activate astrocytes, induced the expected decrease in soma size and an increase in proliferative activity in healthy astrocytes indicative of inflammatory activation (Anderson et al., 2014; Pekny & Pekna, 2014). This did not occur in DMD astrocytes, consistent

with them being constitutively in a more reactive state, hence less responsive to LPS/IFNy stimulation than healthy ones. A systemic increase in mediators of inflammation has been reported in DMD patients and defects in blood–brain barrier function have been found in the *mdx* mouse (Nico et al., 2004; Pelosi et al., 2017). Astrocytes can play an important role in reducing neuroinflammation and its potential deleterious effects (Liddelow & Barres, 2017; Pekny & Pekna, 2014). Therefore, it is tempting to speculate that a chronic inability of DMD astrocytes to respond appropriately to inflammatory stimuli, which are possibly abnormally high due to astrocyte impaired control of blood–brain barrier tightness, may contribute to functional impairment in DMD brains (Frigeri et al., 2001; Giocanti-Auregan et al., 2016).

Furthermore, given increasing evidence of astrocyte heterogeneity (Anderson et al., 2014; Liddelow & Barres, 2017), it is also possible, and not mutually exclusive with the above proposition, that due to *DMD* mutations different types of astrocytes preferentially differentiate from DMD and healthy iPSCs. Further support to the hypothesis that mutations in dystrophin affect astrocyte function was lent by their response to oxidative stress induced by H_2O_2 treatment. Lower concentrations of H_2O_2 were required to induce a loss of viability in DMD astrocytes than in healthy astrocytes. This is consistent with increased vulnerability to oxidative stress reported in muscle biopsies and iPSCs from DMD patients (Jelinkova et al., 2019; Petrillo et al., 2017).

The fact that altered morphology and responses to damage reported in our study were shared by all the DMD astrocyte lines tested, but Dp71/Dp40 expression is maintained in DMD52 astrocytes, suggests that the larger isoforms affected in all lines, Dp427 and Dp140, and possibly Dp116, though not expressed at high levels in astrocytes, are responsible for these defects. In depth analysis of each of these isoforms will be required to dissect their specific role(s). Together, our results suggest that normalization of astrocyte function should be considered one of the therapeutic targets in DMD patients.

4.4 | DMD astrocytes exhibit major transcriptional changes

Analysis of transcriptional signatures using RNA sequencing analysis showed a large overlap of differentially expressed genes between two DMD lines (DMD52 and DMD68), consistent with the comparable behavioral and functional changes observed in all the DMD lines tested.

In muscle, dystrophin plays a key role in connecting the cytoskeleton to the extracellular environment. The significant changes identified here in genes involved in cell adhesion and ECM receptor interaction, including a number of ECM proteins, in DMD astrocytes, as well as the morphological changes observed, suggest an important role for dystrophin in modulating intra-extracellular communication also in astrocytes. Down-regulation of cell adhesion gene expression may also contribute to the occurrence of significant loss of DMD, but not control astrocytes upon stimulation at low H_2O_2 concentrations.

Interestingly, both responses of DMD astrocytes to noxious stimuli and the RNA-seq data suggest a role for dystrophin in modulating astrocyte metabolic activity. The altered responses in DMD astrocytes observed in our functional experiments are consistent with the significant up-regulation of GO-terms involved in cell metabolism, such as protein, peptide and amide transport. In addition, defects in metabolic pathways common to both DMD lines are highlighted by the MaREA analysis. Another evidence of altered homeostatic functions in both DMD52 and DMD68 is provided by the evidence of dysregulation of calcium and cAMP signaling pathways detected by KEGG pathway enrichment analysis. Furthermore, this analysis also highlights several pathways that could contribute to the pro-inflammatory phenotype in DMD astrocytes, as indicated by the GFAP protein up-regulation and EAAT1 down-regulation we have observed. This is consistent with reports that mimicking inflammation by exposing astrocytes to activated microglia or TNFalpha, an inflammatory cytokine released from activated microglia, results in EAAT1 down-regulation (Dumont et al., 2014; Takaki et al., 2012). Also PADI2, a calcium-dependent enzyme known to be expressed in the developing human brain, which has been implicated in a range of inflammatory and neurodegenerative diseases, is up-regulated in DMD astrocytes (Jang et al., 2013; Kin Pong et al., 2014; Wu et al., 2020). Finally, in agreement with results reported by Patel et al. (2019), we show here that GO terms involved in neuronal differentiation are down-regulated, suggesting that DMD astrocytes provide a less supportive environment to neurons and could be implicated in neurodevelopmental deficits. Altogether, our transcriptional analysis has shown that loss of dystrophin in astrocytes significantly impairs several key pathways, which could potentially lead to abnormal interactions of astrocytes with different cell types in the brain, such as neurones and endothelial cells of blood vessels, hence affect brain homeostasis and function. This will deserve in depth investigation.

While here we have focused on transcriptional and protein expression changes common to all DMD lines studied, which could underpin the functional defects observed, some significant differences in gene expression between DMD52 and DMD68 astrocytes were also noted. Future analysis of these differences will be crucial to shed light on the functions of different dystrophin isoform in the nervous system and in patients carrying different dystrophin mutations.

4.5 | Conclusions

Together, the predominance of the shorter dystrophin isoforms observed in the human developing brain is consistent with studies suggesting an association between mutations in the shorter isoforms and brain comorbidities that characterize a significant proportion of DMD patients. However, the abnormal responses to damage in DMD astrocytes identified here appear to be mainly due to the larger isoforms. Importantly, this study has further highlighted that astrocyte function is affected in DMD astrocytes, hence this may contribute to the aforementioned comorbidities. Therefore, to ameliorate neural impairments in DMD patients, therapies should also target these cells. Significantly, given the complexity of dystrophin isoforms, precisely mapping their preferential expression in different human neural cell types and assessing their intracellular distribution and interacting proteins will be crucial to better understanding the role of dystrophin in the human brain.

ACKNOWLEDGMENTS

This work was supported by Newlife Foundation, the UK Medical Research Council (DTI Studentship to OG), EBiSC (IMI joint undertaking no. 115582), GOSH National Institute for Health Research (NIHR) Great Ormond Street Hospital Biomedical Research Centre and the Saudi Arabian Cultural Bureau and Ministry of Education (scholarship to RA). The human embryonic and fetal material was provided by the Human Developmental Biology Resource (http://hdbr.org) jointly funded by the Medical Research Council (grant G070089) and The Wellcome Trust (grant GR082557). F.S.T. is funded by the European Research Council (759108 – HISTOID), the NIHR (CL-2018-18-008) and the Francis Crick Institute which receives its core funding from Cancer Research UK, the UK Medical Research Council and the Wellcome Trust (FC001002). The authors also thank Mr Pierpaolo Ala and the MRC Centre for Neuromuscular Diseases for the support through the Neuromuscular Disease BioBank, and the Muscular Dystrophy UK for its support to G.F., F.S.T. and the Dubowitz Neuromuscular Centre at UCL. We are grateful to Dr Dale Molding at the ICH Microscopy Facility for his advice on acquisition and analysis of the results. We would also like to thank Meera Desai, Jinhong Meng, Jennifer Morgan, Silvia Torelli and Sarah Tabrizi for helpful comments and for sharing some cells and reagents. The views expressed are those of the author(s) and not necessarily those of the NHS, the NIHR or the Department of Health. [Correction added on 22 November 2021, after first online publication: grant number has been updated for European Research Council]

CONFLICT OF INTEREST

The authors declare no conflict of interest.

AUTHOR CONTRIBUTIONS

Jenny Lange designed and performed experiments, analyzed data and drafted the manuscript; Olivia Gillham generated iPSCs, provided feedback and critical reading of the manuscript and generated heatmaps, Reem Alkharji performed experiments and provided feed-back on the manuscript, Giulia Ferrari and Monika Madej generated iPSCs, Michael Flower contributed to RNA-seq analysis, Francesco Muntoni and Francesco Saverio Tedesco obtained funding and provided feed-back and critical reading of the manuscript, Patrizia Ferretti planned research, analyzed data, obtained funding, and wrote the manuscript.

DATA AVAILABILITY STATEMENT

The data that support the findings of this study are stored in local repositories and available from the corresponding author upon reasonable request.

ORCID

Patrizia Ferretti https://orcid.org/0000-0002-3590-6772

REFERENCES

Aartsma-Rus, A., Ginjaar, I. B., & Bushby, K. (2016). The importance of genetic diagnosis for Duchenne muscular dystrophy. *Journal of Medical Genetics*, *53*(3), 145–151. https://doi.org/10.1136/jmedgenet-2015-103387

Akther, S., & Hirase, H. (2021). Assessment of astrocytes as a mediator of memory and learning in rodents. *Glia*. https://doi.org/10.1002/glia.24099. Online ahead of print.

Anderson, M. A., Ao, Y., & Sofroniew, M. V. (2014). Heterogeneity of reactive astrocytes. *Neuroscience Letters*, *565*, 23–29. https://doi.org/10.1016/j.neulet.2013.12.030

Annese, T., Corsi, P., Ruggieri, S., Tamma, R., Marinaccio, C., Picocci, S., Errede, M., Specchia, G., De Luca, A., Frassanito, M. A., Desantis, V., Vacca, A., Ribatti, D., & Nico, B. (2016). Isolation and characterization of neural stem cells from dystrophic mdx mouse. *Experimental Cell Research*, *343*(2), 190–207. https://doi.org/10.1016/j.yexcr.2016.03.019

Aragon, J., Gonzalez-Reyes, M., Romo-Yanez, J., Vacca, O., Aguilar-Gonzalez, G., Rendon, A., Vaillend, C., & Montanez, C. (2018). Dystrophin Dp71 isoforms are differentially expressed in the mouse brain and retina: Report of New alternative splicing and a novel nomenclature for Dp71 isoforms. *Molecular Neurobiology*, *1376-1386*, 1376–1386. https://doi.org/10.1007/s12035-017-0405-x

Bagdatlioglu, E., Porcari, P., Greally, E., Blamire, A. M., & Straub, V. W. (2020). Cognitive impairment appears progressive in the mdx mouse. *Neuromuscular Disorders*, *30*(5), 368–388. https://doi.org/10.1016/j.nmd.2020.02.018

Barnabei, M. S., Sjaastad, F. V., Townsend, D., Bedada, F. B., & Metzger, J. M. (2015). Severe dystrophic cardiomyopathy caused by the enteroviral protease 2A-mediated C-terminal dystrophin cleavage fragment. *Science Translational Medicine*, *7*(294), 294ra106. https://doi.org/10.1126/scitranslmed.aaa4804

Belanger, M., Allaman, I., & Magistretti, P. J. (2011). Brain energy metabolism: Focus on astrocyte-neuron metabolic cooperation. *Cell Metabolism*, *14*(6), 724–738. https://doi.org/10.1016/j.cmet.2011.08.016

Blake, D. J., Weir, A., Newey, S. E., & Davies, K. E. (2002). Function and genetics of dystrophin and dystrophin-related proteins in muscle. *Physiological Reviews*, *82*(2), 291–329. https://doi.org/10.1152/physrev.00028.2001

Brown, M. (1975). A method for combining non-independent, one-sided tests of significance. *Biometrics*, *31*, 987–992.

Chaussenot, R., Amar, M., Fossier, P., & Vaillend, C. (2018). Dp71-dystrophin deficiency alters prefrontal cortex excitation-inhibition balance and executive functions. *Molecular Neurobiology*, *56*, 2670–2684. https://doi.org/10.1007/s12035-018-1259-6

Dai, H., Leeder, J. S., & Cui, Y. (2014). A modified generalized fisher method for combining probabilities from dependent tests. *Frontiers in Genetics*, *5*, 32. https://doi.org/10.3389/fgene.2014.00032

Damiani, C., Di Filippo, M., Pescini, D., Maspero, D., Colombo, R., & Mauri, G. (2017). popFBA: Tackling intratumour heterogeneity with flux balance analysis. *Bioinformatics*, *33*(14), i311–i318. https://doi.org/10.1093/bioinformatics/btx251

Damiani, C., Rovida, L., Maspero, D., Sala, I., Rosato, L., Di Filippo, M., Pescini, D., Graudenzi, A., Antoniotti, M., & Mauri, G. (2020). MaREA4Galaxy: Metabolic reaction enrichment analysis and visualization of RNA-seq data within Galaxy. *Computational and Structural Biotechnology Journal*, *18*, 993–999. https://doi.org/10.1016/j.csbj.2020.04.008

Daoud, F., Angeard, N., Demerre, B., Martie, I., Benyaou, R., Leturcq, F., Cossée, M., Deburgrave, N., Saillour, Y., Tuffery, S., Urtizberea, A., Toutain, A., Echenne, B., Frischman, M., Mayer, M., Desguerre, I., Estournet, B., Réveillère, C., Penisson-Besnier, C. J. M., … Chelly, J. (2009). Analysis of Dp71 contribution in the severity of mental retardation through comparison of Duchenne and Becker patients differing by mutation consequences on Dp71 expression. *Human Molecular Genetics*, *18*(20), 3779–3794. https://doi.org/10.1093/hmg/ddp320

Di Filippo, M., Colombo, R., Damiani, C., Pescini, D., Gaglio, D., Vanoni, M., Alberghina, L., & Mauri, G. (2016). Zooming-in on cancer metabolic rewiring with tissue specific constraint-based models. *Computational*

Biology and Chemistry, *62*, 60–69. https://doi.org/10.1016/j.compbiolchem.2016.03.002

Doorenweerd, N., Dumas, E. M., Ghariq, E., Schmid, S., Straathof, C. S., Roest, A. A., Wokke, B. H., van Zwet, E. W., Webb, A. G., Hendriksen, J. G., van Buchem, M. A., Verschuuren, J. J., Asllani, I., Niks, E. H., van Osch, M. J., & Kan, H. E. (2017). Decreased cerebral perfusion in Duchenne muscular dystrophy patients. *Neuromuscular Disorders*, *27*(1), 29–37. https://doi.org/10.1016/j.nmd.2016.10.005

Doorenweerd, N., Mahfouz, A., van Putten, M., Kaliyaperumal, R., Pac, T. H., Hendriksen, J. G. M., Aartsma-Rus, A. M., Verschuuren, J. J. G. M., Niks, E. H., Reinders, M. J. T., Kan, H. E., & Lelieveldt, B. P. F. (2017). Timing and localization of human dystrophin isoform expression provide insights into the cognitive phenotype of Duchenne muscular dystrophy. *Scientific Reports*, *7*(1), 12575. https://doi.org/10.1038/s41598-017-12981-5

Dumont, A. O., Goursaud, S., Desmet, N., & Hermans, E. (2014). Differential regulation of glutamate transporter subtypes by pro-inflammatory cytokine TNF-alpha in cortical astrocytes from a rat model of amyotrophic lateral sclerosis. *PLoS One*, *9*(5), e97649. https://doi.org/10.1371/journal.pone.0097649

Eide, P. K., & Hansson, H. A. (2017). Astrogliosis and impaired aquaporin-4 and dystrophin systems in idiopathic normal pressure hydrocephalus. *Neuropathology and Applied Neurobiology*, *44*, 474–490. https://doi.org/10.1111/nan.12420

Ferrari, G., Muntoni, F., & Tedesco, F. S. (2020). Generation of two genomic-integration-free DMD iPSC lines with mutations affecting all dystrophin isoforms and potentially amenable to exon-skipping. *Stem Cell Research*, *43*, 101688. https://doi.org/10.1016/j.scr.2019.101688

FitzPatrick, L. M., Hawkins, K. E., Delhove, J., Fernandez, E., Soldati, C., Bullen, L. F., Nohturfft, A., Waddington, S., Medina, D., Bolaños, J., & McKay, T. R. (2018). NF-kappaB activity initiates human ESC-derived neural progenitor cell differentiation by inducing a metabolic maturation program. *Stem Cell Reports*, *10*(6), 1766–1781. https://doi.org/10.1016/j.stemcr.2018.03.015

Frigeri, A., Nicchia, G. P., Nico, B., Quondamatteo, F., Herken, R., Roncali, L., & Svelto, M. (2001). Aquaporin-4 deficiency in skeletal muscle and brain of dystrophic mdx mice. *The FASEB Journal*, *15*(1), 90–98. https://doi.org/10.1096/fj.00-0260com

Fujimoto, T., Yaoi, T., Fushiki, S., & Itoh, K. (2017). Dp71 is regulated by phosphorylation and ubiquitin-proteasome system in neuronal cells. *Biochemical and Biophysical Research Communications*, *492*(3), 349–355. https://doi.org/10.1016/j.bbrc.2017.08.108

Giocanti-Auregan, A., Vacca, O., Benard, R., Cao, S., Siqueiros, L., Montanez, C., Paques, M., Sahel, J. A., Sennlaub, F., Guillonneau, X., Rendon, A., & Tadayoni, R. (2016). Altered astrocyte morphology and vascular development in dystrophin-Dp71-null mice. *Glia*, *64*(5), 716–729. https://doi.org/10.1002/glia.22956

Goodyear, M. J., Junghans, B. M., Giummarra, L., Murphy, M. J., Crewther, D. P., & Crewther, S. G. (2008). A role for aquaporin-4 during induction of form deprivation myopia in chick. *Molecular Vision*, *14*, 298–307.

Graudenzi, A., Maspero, D., Di Filippo, M., Gnugnoli, M., Isella, C., Mauri, G., Medico, E., Antoniotti, M., Damiani, C. (2018). Integration of transcriptomic data and metabolic networks in cancer samples reveals highly significant prognostic power. *Journal of Biomedical Informatics*, *87*, 37–49. https://doi.org/10.1016/j.jbi.2018.09.010

Hawkins, K. E., Joy, S., Delhove, J. M., Kotiadis, V. N., Fernandez, E., Fitzpatrick, L. M., Whiteford, J. R., King, P. J., Bolanos, J. P., Duchen, M. R., Waddington, S. N., & McKay, T. R. (2016). NRF2 orchestrates the metabolic shift during induced pluripotent stem cell reprogramming. *Cell Reports*, *14*(8), 1883–1891. https://doi.org/10.1016/j.celrep.2016.02.003

Hendriksen, R. G. F., Schipper, S., Hoogland, G., Schijns, O. E., Dings, J. T., Aalbers, M. W., & Vles, J. S. (2016). Dystrophin distribution and expression in human and experimental temporal lobe epilepsy. *Frontiers in Cellular Neuroscience*, *10*, 174. https://doi.org/10.3389/fncel.2016.00174

Hendriksen, R. G. F., Vles, J. S. H., Aalbers, M. W., Chin, R. F. M., & Hendriksen, J. G. M. (2018). Brain-related comorbidities in boys and men with Duchenne muscular dystrophy: A descriptive study. *European Journal of Paediatric Neurology*, *22*(3), 488–497. https://doi.org/10.1016/j.ejpn.2017.12.004

Hoogland, G., Hendriksen, R. G. F., Slegers, R. J., Hendriks, M. P. H., Schijns, O., Aalbers, M. W., & Vles, J. S. H. (2018). The expression of the distal dystrophin isoforms Dp140 and Dp71 in the human epileptic hippocampus in relation to cognitive functioning. *Hippocampus*, *29*, 102–110. https://doi.org/10.1002/hipo.23015

Imamura, M., & Ozawa, E. (1998). Differential expression of dystrophin isoforms and utrophin during dibutyryl-cAMP-induced morphological differentiation of rat brain astrocytes. *Proceedings of the National Academy of Sciences of the United States of America*, *95*(11), 6139–6144.

Jang, B., Ishigami, A., Maruyama, N., Carp, R. I., Kim, Y. S., & Choi, E. K. (2013). Peptidylarginine deiminase and protein citrullination in prion diseases: Strong evidence of neurodegeneration. *Prion*, *7*(1), 42–46. https://doi.org/10.4161/pri.22380

Jelinkova, S., Fojtik, P., Kohutova, A., Vilotic, A., Markova, L., Pesl, M., Jurakova, T., Kruta, M., Vrbsky, J., Gaillyova, R., Valášková, I., Frák, I., Lacampagne, A., Forte, G., Dvorak, P., Meli, A. C., & Rotrekl, V. (2019). Dystrophin deficiency leads to genomic instability in human pluripotent stem cells via NO synthase-induced oxidative stress. *Cell*, *8*(1), 53. https://doi.org/10.3390/cells8010053

Jones, V. C., Atkinson-Dell, R., Verkhratsky, A., & Mohamet, L. (2017). Aberrant iPSC-derived human astrocytes in Alzheimer's disease. *Cell Death & Disease*, *8*(3), e2696. https://doi.org/10.1038/cddis.2017.89

Juan-Mateu, J., Gonzalez-Quereda, L., Rodriguez, M. J., Baena, M., Verdura, E., Nascimento, A., Ortez, C., Baiget, M., & Gallano, P. (2015). DMD mutations in 576 Dystrophinopathy families: A step forward in genotype-phenotype correlations. *PLoS One*, *10*(8), e0135189. https://doi.org/10.1371/journal.pone.0135189

Katz, S., Song, J., Webb, K. P., Lounsbury, N. W., Bryant, C. E., & Fraser, I. D. C. (2021). SIGNAL: A web-based iterative analysis platform integrating pathway and network approaches optimizes hit selection from genome-scale assays. *Cell Systems*, *12*(4), 338–352 e335. https://doi.org/10.1016/j.cels.2021.03.001

Kawaguchi, T., Niba, E. T. E., Rani, A. Q. M., Onishi, Y., Koizumi, M., Awano, H., Matsumoto, M., Nagai, M., Yoshida, S., Sakakibara, S., Maeda, N., Sato, O., Nishio, H., Matsuo, M., & Matsuo, M. (2018). Detection of dystrophin Dp71 in human skeletal muscle using an automated capillary Western assay system. *International Journal of Molecular Sciences*, *19*(6), 1546. https://doi.org/10.3390/ijms19061546

Lam, T. A., Man, N. T., & Morris, G. E. (2014). Monoclonal antibodies for clinical trials of Duchenne muscular dystrophy therapy. *Neuromuscular Disorders*, *24*(3), 195–200. https://doi.org/10.1016/j.nmd.2013.11.016

Lange, J., Haslett, L. J., Lloyd-Evans, E., Pocock, J. M., Sands, M. S., Williams, B. P., & Cooper, J. D. (2018). Compromised astrocyte function and survival negatively impact neurons in infantile neuronal ceroid lipofuscinosis. *Acta Neuropathologica Communications*, *6*(1), 74. https://doi.org/10.1186/s40478-018-0575-4

Li, D., Liu, X., Liu, T., Liu, H., Tong, L., Jia, S., & Wang, Y. F. (2020). Neurochemical regulation of the expression and function of glial fibrillary acidic protein in astrocytes. *Glia*, *68*(5), 878–897. https://doi.org/10.1002/glia.23734

Liddelow, S. A., & Barres, B. A. (2017). Reactive astrocytes: Production, function, and therapeutic potential. *Immunity*, *46*(6), 957–967. https://doi.org/10.1016/j.immuni.2017.06.006

Mahyoob Rani, A. Q., Maeta, K., Kawaguchi, T., Awano, H., Nagai, M., Nishio, H., & Matsuo, M. (2019). Schwann cell-specific Dp116 is expressed in glioblastoma cells, revealing two novel DMD gene splicing patterns. *Biochemistry and Biophysics Reports*, *20*, 100703. https://doi.org/10.1016/j.bbrep.2019.100703

Matsuo, M., Awano, H., Matsumoto, M., Nagai, M., Kawaguchi, T., Zhang, Z., & Nishio, H. (2017). Dystrophin Dp116: A yet to be investigated product of the Duchenne muscular dystrophy gene. *Genes (Basel)*, *8*(10), 251. https://doi.org/10.3390/genes8100251

Morris, G. E., Nguyen, C., & Nguyen thi, M. (1995). Specificity and VH sequence of two monoclonal antibodies against the N-terminus of dystrophin. *The Biochemical Journal*, *309*(Pt 1), 355–359. https://doi.org/10.1042/bj3090355

Muntoni, F., Torelli, S., & Ferlini, A. (2003). Dystrophin and mutations: One gene, several proteins, multiple phenotypes. *The Lancet. Neurology*, *2*(12), 731–740.

Nico, B., Paola Nicchia, G., Frigeri, A., Corsi, P., Mangieri, D., Ribatti, D., Svelto, M., & Roncali, L. (2004). Altered blood-brain barrier development in dystrophic MDX mice. *Neuroscience*, *125*(4), 921–935. https://doi.org/10.1016/j.neuroscience.2004.02.008

O'Regan, G. C., Farag, S. H., Casey, C. S., Wood-Kaczmar, A., Pocock, J. M., Tabrizi, S. J., & Andre, R. (2021). Human Huntington's disease pluripotent stem cell-derived microglia develop normally but are abnormally hyper-reactive and release elevated levels of reactive oxygen species. *Journal of Neuroinflammation*, *18*(1), 94. https://doi.org/10.1186/s12974-021-02147-6

Pane, M., Lombardo, M. E., Alfieri, P., D'Amico, A., Bianco, F., Vasco, G., Piccini, G., Mallardi, M., Romeo, D. M., Ricotti, V., Ferlini, A., Gualandi, F., Vicari, S., Bertini, E., Berardinelli, A., & Mercuri, E. (2012). Attention deficit hyperactivity disorder and cognitive function in Duchenne muscular dystrophy: Phenotype-genotype correlation. *The Journal of Pediatrics*, *161*(4), 705–709 e701. https://doi.org/10.1016/j.jpeds.2012.03.020

Patel, A. M., Wierda, K., Thorrez, L., van Putten, M., De Smedt, J., Ribeiro, L., Tricot, T., Gajjar, M., Duelen, R., Van Damme, P., De Waele, L., Goemans, N., Winter, C. T.-d., Costamagna, D., Aartsma-Rus, A., van Duyvenvoorde, H., Sampaolesi, M., Buyse, G. M., & Verfaillie, C. M. (2019). Dystrophin deficiency leads to dysfunctional glutamate clearance in iPSC derived astrocytes. *Translational Psychiatry*, *9*(1), 200. https://doi.org/10.1038/s41398-019-0535-1

Pekny, M., & Pekna, M. (2014). Astrocyte reactivity and reactive astrogliosis: Costs and benefits. *Physiological Reviews*, *94*(4), 1077–1098. https://doi.org/10.1152/physrev.00041.2013

Pekny, M., Pekna, M., Messing, A., Steinhauser, C., Lee, J. M., Parpura, V., Hol, E. M., Sofroniew, M. V., & Verkhratsky, A. (2016). Astrocytes: a central element in neurological diseases. *Acta Neuropathologica*, *131*(3), 323–345. https://doi.org/10.1007/s00401-015-1513-1

Pelosi, L., Forcina, L., Nicoletti, C., Scicchitano, B. M., & Musaro, A. (2017). Increased circulating levels of Interleukin-6 induce perturbation in redox-regulated signaling cascades in muscle of dystrophic mice. *Oxidative Medicine and Cellular Longevity*, *2017*, 1987218–10. https://doi.org/10.1155/2017/1987218

Petrillo, S., Pelosi, L., Piemonte, F., Travaglini, L., Forcina, L., Catteruccia, M., Petrini, S., Verardo, M., D'Amico, A., Musarò, A., & Bertini, E. (2017). Oxidative stress in Duchenne muscular dystrophy: Focus on the NRF2 redox pathway. *Human Molecular Genetics*, *26*(14), 2781–2790. https://doi.org/10.1093/hmg/ddx173

Kin Pong, U., Subramanian, V., Nicholas, A. P., Thompson, P. R., & Ferretti, P. (2014). Modulation of calcium-induced cell death in human neural stem cells by the novel peptidylarginine deiminase-AIF pathway. *BBA Mol Cell Res*, *1843*(6), 1162–1171. https://doi.org/10.1016/j.bbamcr.2014.02.018

Rani, A. Q. M., Farea, M., Maeta, K., Kawaguchi, T., Awano, H., Nagai, M., Nishio, H., & Matsuo, M. (2019). Identification of the shortest splice variant of Dp71, together with five known variants, in glioblastoma cells. *Biochemical and Biophysical Research Communications*, *508*(2), 640–645. https://doi.org/10.1016/j.bbrc.2018.11.168

Relizani, K., Griffith, G., Echevarria, L., Zarrouki, F., Facchinetti, P., Vaillend, C., Leumann, C., Garcia, L., & Goyenvalle, A. (2017). Efficacy and safety profile of Tricyclo-DNA antisense oligonucleotides in Duchenne muscular dystrophy mouse model. *Molecular Therapy—Nucleic Acids*, *8*, 144–157. https://doi.org/10.1016/j.omtn.2017.06.013

Ricotti, V., Mandy, W. P., Scoto, M., Pane, M., Deconinck, N., Messina, S., Mercuri, E., Skuse, D. H., & Muntoni, F. (2016). Neurodevelopmental, emotional, and behavioural problems in Duchenne muscular dystrophy in relation to underlying dystrophin gene mutations. *Developmental Medicine and Child Neurology*, *58*(1), 77–84. https://doi.org/10.1111/dmcn.12922

Sekiguchi, M., Zushida, K., Yoshida, M., Maekawa, M., Kamichi, S., Yoshida, M., Sahara, Y., Yuasa, S., Takeda, S.'i., & Wada, K. (2009). A deficit of brain dystrophin impairs specific amygdala GABAergic transmission and enhances defensive behaviour in mice. *Brain*, *132*(Pt 1), 124–135. https://doi.org/10.1093/brain/awn253

Sheng, W., Zong, Y., Mohammad, A., Ajit, D., Cui, J., Han, D., Hamilton, J. L., Simonyi, A., Sun, A. Y., Gu, Z., Hong, J.-S., Weisman, G. A., & Sun, G. Y. (2011). Pro-inflammatory cytokines and lipopolysaccharide induce changes in cell morphology, and upregulation of ERK1/2, iNOS and sPLA(2)-IIA expression in astrocytes and microglia. *Journal of Neuroinflammation*, *8*, 121. https://doi.org/10.1186/1742-2094-8-121

Sofroniew, M. V., & Vinters, H. V. (2010). Astrocytes: Biology and pathology. *Acta Neuropathologica*, *119*(1), 7–35. https://doi.org/10.1007/s00401-009-0619-8

Sun, Y., Pollard, S., Conti, L., Toselli, M., Biella, G., Parkin, G., Willatt, L., Falk, A., Cattaneo, E., & Smith, A. (2008). Long-term tripotent differentiation capacity of human neural stem (NS) cells in adherent culture. *Molecular and Cellular Neurosciences*, *38*(2), 245–258.

Tadayoni, R., Rendon, A., Soria-Jasso, L. E., & Cisneros, B. (2012). Dystrophin dp71: The smallest but multifunctional product of the duchenne muscular dystrophy gene. *Molecular Neurobiology*, *45*(1), 43–60. https://doi.org/10.1007/s12035-011-8218-9

Takaki, J., Fujimori, K., Miura, M., Suzuki, T., Sekino, Y., & Sato, K. (2012). L-glutamate released from activated microglia downregulates astrocytic L-glutamate transporter expression in neuroinflammation: The 'collusion' hypothesis for increased extracellular L-glutamate concentration in neuroinflammation. *Journal of Neuroinflammation*, *9*, 275. https://doi.org/10.1186/1742-2094-9-275

Tsao, C. Y., & Mendell, J. R. (2006). Coexisting muscular dystrophies and epilepsy in children. *Journal of Child Neurology*, *21*(2), 148–150. https://doi.org/10.1177/08830738060210021601

Vagaska, B., Gillham, O., & Ferretti, P. (2020). Modelling human CNS injury with human neural stem cells in 2- and 3-dimensional cultures. *Scientific Reports*, *10*(1), 6785. https://doi.org/10.1038/s41598-020-62906-y

Vagaska, B., New, S. E., Alvarez-Gonzalez, C., D'Acquisto, F., Gomez, S. G., Bulstrode, N. W., Madrigal, A., & Ferretti, P. (2016). MHC-class-II are expressed in a subpopulation of human neural stem cells in vitro in an IFNgamma-independent fashion and during development. *Scientific Reports*, *6*, 24251. https://doi.org/10.1038/srep24251

Vaillend, C., & Chaussenot, R. (2017). Relationships linking emotional, motor, cognitive and GABAergic dysfunctions in dystrophin-deficient mdx mice. *Human Molecular Genetics*, *26*(6), 1041–1055. https://doi.org/10.1093/hmg/ddx013

van den Bergen, J. C., Wokke, B. H., Janson, A. A., van Duinen, S. G., Hulsker, M. A., Ginjaar, H. B., **van** Deutekom JC, Aartsma-Rus A, Kan HE Verschuuren, J. J. (2014). Dystrophin levels and clinical severity in Becker muscular dystrophy patients. *Journal of Neurology, Neurosurgery, and Psychiatry*, *85*(7), 747–753. doi:https://doi.org/10.1136/jnnp-2013-306350

Waite, A., Brown, S. C., & Blake, D. J. (2012). The dystrophin-glycoprotein complex in brain development and disease. *Trends in Neurosciences*, *35*(8), 487–496. https://doi.org/10.1016/j.tins.2012.04.004

Wilson, D. J. (2019). The harmonic mean p-value for combining dependent tests. *Proceedings of the National Academy of Sciences of the*

United States of America, *116*(4), 1195–1200. https://doi.org/10.1073/pnas.1814092116

Wingeier, K., Giger, E., Strozzi, S., Kreis, R., Joncourt, F., Conrad, B., Gallati, S., & Steinlin, M. (2011). Neuropsychological impairments and the impact of dystrophin mutations on general cognitive functioning of patients with Duchenne muscular dystrophy. *Journal of Clinical Neuroscience*, *18*(1), 90–95. https://doi.org/10.1016/j.jocn.2010.07.118

Wu, Z., Deng, Q., Pan, B., Alam, H. B., Tian, Y., Bhatti, U. F., Liu, B., Mondal, S., Thompson, P. R., & Li, Y. (2020). Inhibition of PAD2 improves survival in a mouse model of lethal LPS-induced endotoxic shock. *Inflammation*, *43*(4), 1436–1445. https://doi.org/10.1007/s10753-020-01221-0

SUPPORTING INFORMATION

Additional supporting information may be found in the online version of the article at the publisher's website.

How to cite this article: Lange, J., Gillham, O., Alkharji, R., Eaton, S., Ferrari, G., Madej, M., Flower, M., Tedesco, F. S., Muntoni, F., & Ferretti, P. (2021). Dystrophin deficiency affects human astrocyte properties and response to damage. *Glia*, 1–25. https://doi.org/10.1002/glia.24116